On the optical counterparts of radio transients and variables

A. J. Stewart, 1,2,3 * T. Muñoz-Darias, 4,5,2,3 R. P. Fender^{2,3} and M. Pietka^{2,3}

- Sydney Institute for Astronomy, School of Physics, The University of Sydney, NSW 2006, Australia
- ² Astrophysics, Department of Physics, University of Oxford, Keble Road, Oxford OX1 3RH, UK
- ³ Physics and Astronomy, University of Southampton, Highfield, Southampton, SO17 1BJ, UK
- ⁴ Instituto de Astrofísica de Canarias, 38200 La Laguna, Tenerife, Spain
- ⁵ Departamento de astrofísica, Univ. de La Laguna, E-38206 La Laguna, Tenerife, Spain

Accepted 2018 June 20. Received 2018 June 20; in original form 2017 September 29

ABSTRACT

We investigate the relation between the radio (F_r) and optical (F_0) flux densities of a variety of classes of radio transients and variables, with the aim of analysing whether this information can be used, in the future, to classify such events. Using flux density values between 1–10 GHz and the optical bands V and R, we build a sample with a total of 12,441 F_r and F_o measurements. The sample contains both Galactic objects, such as stellar sources and X-ray binaries, and extragalactic objects, such as gamma-ray bursts and quasars. By directly comparing the two parameters, it is already possible to distinguish between the Galactic and extragalactic populations. Although individual classes are harder to separate from the F_r - F_o parameter space to a high accuracy, and can only provide approximations, the basic approach provides an already useful foundation to develop a more accurate classification technique. In addition, we illustrate how example objects from different classes move in the parameter space as they evolve over time, offering a feature that could be used to reduce the confusion between classes. A small, blind test of the classification performance is also undertaken using a catalogue of FIRST transient and variable sources, to demonstrate the advantages and current limitations of the approach. With more multi-wavelength data becoming available in the future, we discuss other classification techniques which the F_r - F_0 method could be combined with and potentially become an important part of an automatic radio transient classification system.

Key words: radio continuum: general – radio continuum: transients – stars: variables: general – stars: statistics – galaxies: statistics – quasars: general

INTRODUCTION

The next generation of radio telescopes will survey the radio sky to unprecedented levels. This has the potential to uncover a wide variety of radio transient and variable phenomena, from both expected, and unexpected, origins. In recent years various large area surveys dedicated to searching for such radio sources have been carried out (e.g., Ofek et al. 2011; Williams et al. 2013; Rowlinson et al. 2016; Mooley et al. 2016) with some utilising the first wave of new instruments such as the upgraded Karl G. Jansky Very Large Array (VLA; Perley et al. 2011), and at low frequencies, the Low Frequency Array (LOFAR; van Haarlem et al. 2013) and the Murchison Widefield Array (MWA; Tingay et al. 2013). These will shortly be joined by a group of new cen-

timetre wavelength instruments such as MeerKAT (Booth & Jonas 2012), ASKAP (Johnston et al. 2008) and Apertif/WSRT (Oosterloo, Verheijen & van Cappellen 2010). Lastly, the Square Kilometre Array (SKA; Dewdney et al. 2009) in the 2020s, has the potential to uncover thousands of transients (Metzger, Williams & Berger 2015; Fender et al. 2015). At optical wavelengths, surveys such as the Palomar Transient Factory (PTF; Rahmer et al. 2008; Rau et al. 2009; Law et al. 2009) and those using the Pan-STARRS1 telescope (Tonry et al. 2012) have produced a high yield of transient sources (e.g. Drout et al. 2014; Cenko et al. 2015, and the Pan-STARRS1 survey for transients currently lists over 10,000 transient sources since 2013¹). The future Large Synoptic Survey Telescope (LSST; Ivezic et al. 2008) will view the optical sky to an unprecedented level of detail. The

^{*} email:adam.stewart@sydney.edu.au

https://star.pst.qub.ac.uk/ps1threepi/psdb/

quality of images combined with a fast survey speed and a wide field of view could result in an estimated 10 million events per night (Bloom et al. 2012; Kantor 2014).

Our aim in this paper is to produce an initial analysis of the photometric properties of radio transients and variables along with their optical counterparts - providing a foundation to classify blindly discovered radio sources. In this work we consider radio transients that are found in the image-plane. These are usually incoherent synchrotron events that can be both Galactic, such as flare stars (though flare stars largely start to be dominated by coherent emission 5 GHz; Bastian 1990), and extragalactic such as gammaray bursts and supernovae (we refer the reader to Metzger et al. 2015 and Fender et al. 2015 for reviews of radio transient sources). We also consider radio pulsars - an example of coherent emission. Historically, a handful of radio transient events have been discovered through blind surveys (e.g. Levinson et al. 2002; Gal-Yam et al. 2006; Ofek et al. 2010; Bower et al. 2007; Frail et al. 2012; Stewart et al. 2016), however, discoveries that are only detected in the radio make identifying the class of the transient object challenging. Although information can be gained from the nature of the radio emission itself, for example the time-scale of the event (Pietka, Fender & Keane 2015), the use of simultaneous or rapid multi-wavelength follow up data becomes crucial in order to establish the type of the transient source in question. This was demonstrated by Mooley et al. (2016) where the authors used various multi-wavelength follow-up, primarily optical in cohesion with PTF, to identify transient and variable sources detected in a 50 deg² pilot survey at 3 GHz with the VLA. On the optical side, we note that we primarily consider optical point-like sources since they account for the vast majority of the variable and transient populations and for the uniformity they offer. Though radio transient sources can appear behind extended optical objects which may offer clues as to their classification, but on the other hand, confirming the association between the two can be challenging.

The likely high number of radio transient events in the SKA era means that detailed follow-up of every event will be implausible. This means that rapid classification techniques will be necessary such as the ones widely utilised in optical surveys (Saglia et al. 2012; Djorgovski et al. 2012). These commonly involve machine learning algorithms based upon light-curve features (Richards et al. 2011) and other measurements such as optical colour (Mahabal et al. 2011). Automatic classification has also been investigated at X-ray wavelengths, e.g. Lo et al. (2014) used random forest algorithms to define a classification of X-ray variable sources based upon features derived from time series, spectra and multi-wavelength catalogue data (also see Farrell, Murphy & Lo 2015). In the radio, attempts have been made to classify objects based upon light-curve features and the previously mentioned time-scale of the event (Rebbapragada et al. 2012; Pietka et al. 2017). However, the need to rapidly classify objects has not been a requirement for radio transient astronomy, with efforts instead focussed on the rapid detection of events. We aim to provide the foundation that will lead to a similar system developed in the radio and optical parameter space.

Our selection of the radio–optical properties is due to the growing number of robotic optical telescopes such as

the Liverpool Telescope (Steele et al. 2004) in the northern hemisphere, SMARTS² in the south, and projects such as the Las Cumbres Observatory Global Telescope Network (Brown et al. 2013). We expect rapid, or simultaneous, optical follow-up to be the most abundant for radio transients. This is in addition to present and future optical catalogues (e.g. the Sloan Digital Sky Survey (SDSS; Eisenstein et al. 2011) and LSST). For rapid classifications we also aim to only use basic properties of observations that are easily obtainable - the raw radio and optical flux density measurements of the observed object that would avoid expensive spectroscopic campaigns for a preliminary classification. A project that is very applicable to the above scenario is the MeerLICHT telescope³. It is a robotically operated 65 cm telescope with a 2 deg² field of view that will follow MeerKAT observations and provide simultaneous optical coverage.

We first construct a sample of radio and optical flux density values of known radio transient and variable objects, which is described in Section 2. This is followed by Section 3 which shows the results that are discussed in Section 4 along with the exploration of the transient diagnostic application of the data. We finish with our conclusions in Section 5.

2 DATA COLLECTION & METHODS

We collected radio and optical flux density measurements of various types of transient objects from the literature. We define these as F_r and F_o respectively throughout this paper. The classes of object for which data were gathered were as follows: quasar, stellar, radio pulsar, cataclysmic variable (CV), X-ray binary (XRB), gamma-ray burst (GRB) and supernova (SN). We only consider detections of objects at both wavelengths and currently include no upper limit values. In cases where no tabled observational data was available, measurements were obtained from light-curve figures using WebPlotDigitizer⁴. We also note that because of how the sample is constructed, i.e. from many different sources, the sample will inevitably be very biased. At this early stage of the project we do not attempt to un-bias the dataset due to the complexity of the task. We discuss such issues in Section 4.

2.1 Measurement selection criteria

Requiring many different classes of objects meant collecting data from a range of projects, all done with different methods, instruments and data quality. Hence, we decided upon following a selection criteria to provide a useful sample in terms of size and quality. In the optical case we concentrated on gathering V and/or R band measurements. The two bands were found to be the most common, and for our

² SMARTS is the Small and Medium Aperture Research Telescope System; see http://www.astro.yale.edu/smarts/.

³ MeerLICHT is a prototype telescope for the BlackGEM telescope array; see http://www.ast.uct.ac.za/meerlicht/MeerLICHT.html.

⁴ Web based tool to extract data from plots, images and maps, authored by Ankit Rohatgi (http://arohatgi.info/WebPlotDigitizer).

purposes were considered valid to be used interchangeably. If both were available then R was used and if only an SDSS-rband measurement was available for a source, we recorded it as R - we assume that the difference is negligible compared to the scatter created by using both V and R. Nearly all optical magnitudes obtained were recorded in the Johnson-Cousins BVRI system, with the exception of optically selected quasars which were gathered from the SDSS survey in the r band, which is considered to be in the AB system, four GRBs and one SN. As the guasars are by far the dominant class and the preference to work in the AB system, we account for this by converting all Johnson-Cousins magnitudes to the AB system using the offsets as defined by Frei & Gunn (1994) (specifically the author's table 2). Any sources that were collected in the SDSS-r filter were not converted. We also do not account for extinction on optical magnitudes to mimic values obtained directly from the telescope.

The $F_{\rm r}$ measurements selected were in the frequency range of 1–10 GHz. Using a large portion of the radio bandwidth meant that the dataset would be useful for a range of common radio frequencies - given the overall aim of providing a classification to radio sources. The large range also meant that a sizeable sample could be created. We believe the range of frequencies does not have a negative effect on our initial investigation as discussed further in Section 4.

In addition, all the populations can experience rapid flux density variations, hence, the timing between the $F_{\rm r}$ and $F_{\rm o}$ measurements was also important. Ideally, simultaneous measurements are required, with our definition of 'simultaneous' for the purposes of this work meaning recorded ≤ 1 d apart. However, while possible with some classes, the data did not exist for others. This is particularly true for quasars and stellar sources due to the use of existing catalogues to obtain the measurements. Simultaneous measurements for pulsars were also found to be too rare, so non-simultaneous measurements were used.

There is also the issue of whether the objects are in a quiescent or transient/flaring state when the flux density measurements are recorded. For example, classes such as GRBs and SN are always in a 'transient' state, where as stellar and quasar sources can be seen as 'quiescent' that can display flaring behaviour. This will create extra biases in our sample, e.g. some classes may be dominated by flaring objects as this is what has originally triggered the observations of the source. Though sources in a flaring state are also those more likely to be discovered as a 'new source' transient object, which are the primary focus of this work. Throughout the description of the sample we clarify what states we believe the sources to be in, or give the exact nature where possible. The two classes where catalogues have been used, the quasars and stellar sources, we assume to be dominated by sources in a quiescent state, as neither catalogue had any selection criteria suggesting otherwise (see the following Sections 2.2 and 2.3). Given that these classes are dominant objects in the sky, we somewhat consider them as a measure of the 'background'. We also attempt to be consistent in our selections of what enters the final result for other classes (e.g. using radio peak measurements for flaring objects) and we also address this issue by exploring how transient objects evolve over time in the F_r and F_o domain (Section 2.8).

The following sections give a summary of data collected for each class of object, with Table 1 showing the final total

Table 1. The total number of pairs of F_r and F_o measurements included in the sample for each class of object. Also shown is the total number of optical colour measurements which were obtained where available as an additional reference for our sample. The potential use of colour is discussed in Section 4.

Object Class	Total No.
Quasar (Optical Sel.)	11,062
Quasar (Radio Sel.)	720
Stellar	534
Radio pulsar	7
CV	18
XRB	26
GRB	48
SN	26
Total	12,441

number of measurements gathered for each class. Where applicable, the references for the individual measurements can be found in Appendix A along with distance measurements, and in the cases of SN and GRB, the age of the transient when the used measurements were recorded. Fig. A1 shows the distributions of the radio frequencies and optical bands used for each class in the sample. In addition, the redshift, or distance, distributions for the large samples of quasars, stellar sources and GRBs are also shown in Figs. A2, A3 and A4 respectively.

2.2 Quasars

We used two different selection methods to populate our quasar sample. First, we selected quasars which had been classified as such through their optical properties, and second, a sample of quasars which had been defined by their radio properties.

2.2.1 Optically selected

Two versions of the SDSS quasar catalogue were used: the Seventh Data Release quasar catalogue (DR7QC; Schneider et al. 2010) and the Ninth Data Release quasar catalogue (DR9QC; Pâris et al. 2012). The DR7QC consisted of data from the SDSS-I and SDSS-II surveys (York et al. 2000) and contains 105,783 entries, where as the DR9QC was compiled using SDSS-III (Eisenstein et al. 2011) and contains 87,822 quasars. The two catalogues contain cross-matches to the VLA FIRST 1.4 GHz survey (resolution of 5".4; White et al. 1997) and record the peak $F_{\rm r}$. These are matches within 2.0" of the SDSS quasar position, and are likely to be cores of the galaxy. If any quasars were present in both the SDSS catalogues, then only the information from the DR9QC was used. In total, 11,062 optically selected quasars are included in our sample.

Combining the two SDSS quasar catalogues provided us with a diverse range of objects, particularly in redshift, z, as this is the main difference between the two. The DR9QC was built using data from the Baryon Oscillation Spectroscopic Survey of SDSS-III (BOSS; Dawson et al. 2013), which targeted over 150,000 z > 2.15 quasars. This resulted in DR9QC containing 2.6 times more quasars at z > 2.15 than the

4 Stewart et al.

DR7QC, for which the majority of quasars were at z < 2.15 (see Fig. A2 for the QSO sample redshift distribution). We note that some of the optical quasars may have been originally identified as such by the presence of a radio counterpart, but for our purposes we define them as 'optically selected'.

We use the r band magnitude from the SDSS survey which we assume to be already in the AB magnitude system hence no conversion is applied. We also note that the 1 mJy limit of the FIRST survey used in this class is a significant limiting factor for the project, however it remains the best source of defining the radio properties of the quasar population. The consequences of the limit are discussed further in Sections 3 & 4 along with how we would expect the population to appear beyond the 1 mJy limit.

2.2.2 Radio selected

The basis of our radio selected sample was the Parkes Catalogue (Wright & Otrupcek 1990), where we selected any object identified as a quasar or a BL Lacertae. For each object, the $F_{\rm r}$ at 5 GHz was obtained (1.4 GHz data was poorly sampled), and using SIMBAD, we gathered V and/or R photometry measurements when available. Assuming a resolution of 3.3 arcmin for Parkes ($D=64~{\rm m}$) at 5 GHz, we assume the total $F_{\rm r}$ is recorded. In total, 720 radio selected quasars were included in the sample.

2.3 Stellar objects

To characterise the Galactic stellar sources, we have used a catalogue of F_0 and F_r properties as used by Güdel (2002) (in particular the information presented in their fig. 1). The radio measurements of this catalogue are in turn based upon stellar radio detections between 1–10 GHz, as reported by Wendker (1995). F_0 measurements in the V band were also obtained by Wendker (1995) from a wide range of sources in the literature at the time. The classes of objects stated in the catalogue were as follows: RS CVn and Algol-type stars; double stars; magnetic stars; BY Dra-type stars; Symbiotic stars; Herbig stars; WR stars; T Tauri stars; PMS stars; and isolated stars. We checked the classifications against the most recent literature and removed any source that were now classed as: X-ray binary; X-ray source; X-ray nova; planetary nebular; QSO; and radio galaxy. We further generalised the subcategories into: Stars, RS CVn, Algol, Young Stellar Objects (YSOs), Variable Stars, Symbiotic Stars and 'other'. CVs were also removed and integrated into the stand-alone CV data (refer to Section 2.5). We note that while we have defined CVs and X-ray binaries as standalone samples, it will be shown in Section 3 that using all the sub-classifications of the stellar sample was not useful.

In total, 534 stellar sources are included. Similar to the quasar sample, using a catalogue approach meant that we can sample all stellar objects in a variety of astrophysical states. We assume this to be true given that no strict selection criteria was imposed by Wendker (1995), in which optical magnitudes were gathered from a wide range of literature sources.

2.4 Isolated neutron stars

2.4.1 Radio pulsars

We have included seven radio pulsars in the sample: Crab pulsar, Vela pulsar, B0540-69, B1509-58, B0656+14, B1133+16 and B0950+08. As simultaneous observations are rare, we have used optical observations of the pulsars performed by Mignani (2011), paired with radio observations that were compiled in the ATNF Pulsar Catalogue (Manchester et al. 2005). The radio measurements are all at 1.4 GHz. Reference details can be found in Table A1.

2.4.2 Other isolated neutron stars

We also attempted to gather measurements for other types of isolated neutron stars such as magnetars and RRATs. As of writing, the McGill Online Magnetar Catalogue (Olausen & Kaspi 2014)⁵ lists four magnetars with radio observations. However, these could not be matched with optical detections and thus were not used. The same is true with RRATs where no optical detections have been made (Dhillon, Marsh & Littlefair 2006; Dhillon et al. 2011).

2.5 Cataclysmic variables

Gathering a sample of CVs in the context of our project is challenging given the dynamic nature of these objects, which can undergo large variations in brightness over relatively short periods of time. While CVs are commonly persistent sources that undergo flaring events, they are likely to be discovered as new transient events when such a flare is detected above the detection limits. Hence, CVs (along with other classes such as XRBs, SN and GRBs) will significantly move around the F_0 – F_r parameter space, a feature that we explore in this work by gathering a dynamic data sample (Section 2.8).

In total, we have included 17 CVs from a range of sources in a conscious attempt to sample the class during quiescence and flaring events. Of these, 7 are from the stellar sample as discussed in Section 2.3. These are T CrB; V* RT Ser; RS Oph; V 4074 Sgr; HM Sge; PU Vul and AG Peg. All are nova type CVs, and the precise timing between the optical and radio observations is unknown, hence we treat these as quiescent measurements (though this is not certain). The 10 other CVs were gathered as follows. Five nova CVs (Nova Sco 2012, T Pyx, V1500 Cyg, V1723 Cyg and V1974 Cyg) were included from the work performed by Pietka et al. (2015) on studying radio light-curve properties of objects, and are all flaring events. Three novalike CVs that were detected by Coppejans et al. (2015) in the radio at 6 GHz (RW Sex, V603 Aql and TT Ari) that are considered as being in quiescence. Although, one measurement of TT Ari showed a radio flare in one of the author's observations, and hence, has two measurements included in the sample. Lastly, two dwarf nova, SS Cyg and V3885 Sgr, where the former is recorded at the radio peak of an outburst, and the latter is a targeted detection and is considered in quiescence. All these measurements are in the frequency

⁵ http://www.physics.mcgill.ca/~pulsar/magnetar/main. html.

range 2.7–8.6 GHz and the known distances for the objects included range 0.12-5.0 kpc. For the sources outside of the stellar sample, if no published F_0 measurements were available, the V or R band magnitudes closest to the date of the radio observations, were obtained from AAVSO⁶ lightcurves. The measurements of the F_0 and F_r of the sources from Pietka et al. (2015) and those of SS Cyg are within 1 d of each other in time. However the V3885 Sgr measurements are not simultaneous, and are separated by 38 d. The time separation between the F_0 and F_r measurements of the Coppejans et al. (2015) sources was 1 yr, 1 d and 22 d for RW Sex, V603 Aql and TT Ar, respectively. In total, 18 pairs of measurements were used for CVs. Reference details can be found in Table A2. Five CVs have been included in the dynamic data sample, of which the details can be found in Table 2 and is discussed in Section 2.8.

2.6 X-ray binaries

Similar to CVs above, the brightness of XRBs can vary by large magnitudes during flare events and numerous measurements are made (though not all) on the basis of an X-ray transient detection. To build the sample we used two catalogues: the Catalogue of high-mass X-ray binaries in the Galaxy (4th edition; Liu, van Paradijs & van den Heuvel 2006) (LiuHMXB) and the Catalogue of low-mass X-ray binaries in the Galaxy, LMC, and SMC (4^{th} edition; Liu, van Paradijs & van den Heuvel 2007) (LiuLMXB). The XRBs with a high confidence radio detection as defined in the catalogues (doubtful radio detections were excluded) along with an optical detection were considered, which meant referring to the literature on the object to determine if there were suitable data. Three types of measurements were used in the sample: (i) radio and optical observations following the discovery of the respective object as an X-ray transient. These observations are commonly performed within days to weeks after the discovery and in this case we record the pair of measurements at the radio peak if possible. (ii) targeted (often in the radio) observations of known XRBs in an attempt to gain a detection, and (iii) long term monitoring (usually at different points in time for radio and optical) for which an average flux density can be recorded. If major flaring occured during the monitoring of the respective source then we did not include the object. Incorporating these different methods also had the advantage of providing a range of measurements over the F_r - F_o parameter space.

In total, 26 XRB objects were included: 6 from LiuH-MXB and 20 from LiuLMXB. The majority of the measurements (19) were within 1 d of each other, with a further four up to 4 d. The final three were 1 week (2) and $\sim\!20$ yr apart (the latter being an average flux density). Reference details for each XRB can be found in Table A3, along with notes of the circumstance of the used observations. These show that the sample is dominated by flaring events at the radio peak as the majority are follow-up observations as described above. The radio measurements span 1–9 GHz and the distance of the objects span 1–27 kpc . Eight of the XRBs were

⁶ American Association of Variable Star Observers; see https://www.aavso.org.

also included in the dynamic data sample of which details can be found in Table 2 and is discussed in Section 2.8.

2.7 Supernovae & Gamma-ray bursts

Our approach for SNe and GRBs was to use the first simultaneous (≤ 1 d) measurements available in the literature. Note that this is not necessarily the first detection measurement available at either wavelength, as these were unlikely to be simultaneous. All the $F_{\rm r}$ and $F_{\rm o}$ measurements included in both samples are ≤ 1 d apart in observation time, with the sample size large enough to avoid including non-simultaneous measurements.

2.7.1 Supernovae

We have used a sample of radio detected core-collapse SNe compiled by Romero-Cañizales et al. (2014). The sample includes a variety of SNe types: Ib, Ic, II, IIn, IIb, IIP and a full list of the 26 SNe can be found in Table A4 along with references and distances. The measurements range from 3–743 d after the reported explosion dates, with a distance range of 3.4–154.0 Mpc (see Fig. A3) and are within the radio frequency range of 4.8–8.6 GHz. From the sample, 15 SNe were also included in the dynamic data sample of which details can be found in Table 2 and is discussed in Section 2.8. The SN sample was compiled with the aid of the valuable resource *The Open Supernova Catalog* (Guillochon et al. 2017).

2.7.2 Gamma-ray bursts

Our GRB sample is based upon a catalogue of radio GRB afterglows that was compiled by Chandra & Frail (2012). We only used GRBs that had simultaneous F_0 and F_Γ measurements available. In total we have recorded measurements for 48 GRBs, with details presented in Table A5. Two of the bursts were short GRBs (defined as SHBs by Chandra & Frail 2012), which were GRB 050724 and GRB 051221A, with the rest characterised as long GRBs. The measurements range from < 1–26 d post burst, and the sample spans a redshift range of 0.03–4.50 (see Fig. A4) and are within the radio frequency range of 1.4–9.0 GHz. Eight GRBs were also included in the dynamic data sample of which details can be found in Table 2 and is discussed in the following Section 2.8.

2.8 Dynamic Data

The $F_{\rm r}$ and $F_{\rm o}$ of objects will change over time. This is an important feature to consider since the property could help to reduce confusion between classes when they overlap in the $F_{\rm r}$ - $F_{\rm o}$ parameter space. In addition, the movement also helps to address the flaring or quiescent bias in the sample by showing an object's full range as opposed to a data point at the peak of a flare. A detailed study of how classes of objects evolve in the $F_{\rm r}$ - $F_{\rm o}$ parameter space is beyond the scope of this initial investigation. Nevertheless, we gathered a dynamic data sample based upon our main sample to explore what could be expected. The sources selected were not dependant on any prior set conditions. We judged each object as the main sample was being collected and used those

6 Stewart et al.

Table 2. The information regarding the sample of dynamic sources we have used in the investigation. The first and last dates of the measurements refer to the F_r measurement. 'Timespan' refers to the total number of days between the first pair of F_r and F_0 measurements and the last. 'No. of data points' refers to the number of simultaneous pairs of F_{Γ} and F_{O} that were obtained. For further details on the specifics of the sample, such as when measurements began relative to the event being detected, please refer to Section 2.8 and Tables A2, A3, A4 and A5. The references are as follows: [1] Eyres et al. (2009), [2] AAVSO, [3] Körding et al. (2008), [4] Nelson et al. (2014), [5] Hjellming et al. (1979), [6] Hjellming (1996), [7] Clark et al. (2000), [8] Shrader et al. (1994), [9] Shaposhnikov et al. (2007), [10] Kalemci et al. (2016), [11] SMARTS (see Buxton et al. 2012), [12] della Valle et al. (1991), [13] Ball et al. (1995), [14] Corbel et al. (2013), [15] Buxton et al. (2012), [16] Han & Hjellming (1992), [17] Casares et al. (1991), [18] Hannikainen et al. (2001), [19] Jain et al. (1999), [20] Brocksopp et al. (2002) (GBI), [21] Uemura et al. (2004), [22] van Dyk et al. (1993), [23] Clocchiatti et al. (2001), [24] Weiler et al. (2007), [25] Richmond et al. (1996b), [26] Weiler et al. (2011), [27] Richmond et al. (1996a), [28] Yokoo et al. (1994), [29] Lee et al. (1995), [30] Kulkarni et al. (1998), [31] Clocchiatti et al. (2011), [32] Berger et al. (2002a), [33] Gal-Yam et al. (2002), [34] Beswick et al. (2005), [35] Tsvetkov et al. (2008), [36] Wellons et al. (2012), [37] Drout et al. (2011), [38] Chevalier et al. (2006), [39] Misra et al. (2007a), [40] Salas et al. (2013), [41] Young et al. (2010), [42] Soderberg et al. (2010b), [43] Hunter et al. (2009), [44] Roy et al. (2013), [45] van der Horst et al. (2011), [46] Mazzali et al. (2008), [47] Roming et al. (2009), [48] Soderberg et al. (2010a), [49] Pignata et al. (2011), [50] Frail et al. (2000b), [51] Sokolov et al. (1998), [52] Galama et al. (2003), [53] Castro-Tirado et al. (2001), [54] Berger et al. (2000), [55] Rhoads & Fruchter (2001), [56] Berger et al. (2003a), [57] Lipkin et al. (2004), [58] Cenko et al. (2006), [59] Soderberg et al. (2006a), [60] Ferrero et al. (2006), [61] Chandra et al. (2008), [62] Moin et al. (2013), [63] Marshall et al. (2011), [64] WEBT Archive, Villata et al. (2009) and [65] GASP-WEBT archive, Raiteri et al. (2011). WEBT is the Whole Earth Blazar Telescope and GASP the GLAST-AGILE Support Program.

Object name	Object class	Date of first flux densities	Date of last flux densities	Timespan (d)	No. of data points	Radio freq. (GHz)	Optical band	Radio ref.	Optical ref.
RS Oph	CV, Nova	2006 Feb 18	2006 Apr 03	45	9	6.0	V	[1]	[2]
SS Cyg	CV, Dwarf Nova	$2007 \; \mathrm{Apr} \; 25$	2007 May 10	15	8	8.6	V	[3]	[3]
T Pyx	CV, Nova	2011 June 19	2012 Sept 07	445	10	5.0	V	[4]	[4]
V1500 Cyg	CV, Nova	1975 Sept 24	1976 Oct 01	373	11	8.1	Vis.	[5]	[2]
V1974 Cyg	CV, Nova	$1992~\mathrm{May}~04$	1994 Sept 14	862	17	5.0	Vis.	[6]	[2]
XTE J0421+560	HMXB	1998 Apr 04	1998 Apr 21	17	11	8.0	R	[7]	[7]
GRO J0422+32	LMXB	1992 Aug 13	1993 Jan 15	155	6	5.0	V	[8]	[8]
GRO J1655-40	LMXB	2005 Feb 20	2005 Apr 05	45	16	4.86	V	[9,10]	[11]
GS 1124-684	LMXB	1991 Jan 18	1991 Jan 31	13	8	4.7	R	[12]	[13]
GX 339-4	LMXB	2011 Feb 06	2011 Apr 27	80	15	9.0	V	[14]	[15]
V404 Cygni	LMXB	1989 May 30	1989 July 04	35	7	8.3	R	[16]	[17]
XTE J1550-564	LMXB	1998 Sept 20	1998 Sept 29	9	7	4.8	R	[18]	[19]
XTE J1859+226	LMXB	1999 Oct 17	1999 Dec 31	74	46	2.25	R	[20]	[21]
SN 1990B	SN, Type Ic	1990 Feb 13	1990 May 29	105	5	5.0	V	[22]	[23]
SN 1993J	SN, Type II	1993 Apr 08	1994 Feb 08	306	34	8.3	R	[24]	[25]
SN 1994I	SN, Type Ic	1994 Apr 03	1994 Aug 08	127	26	8.3	R	[26]	[27,28,29]
SN 1998bw	SN, Type Ic	1998 Apr 28	1998 July 15	78	22	8.64	R	[30]	[31]
SN 2002ap	SN, Type Ic	2002 Feb 01	2002 Feb 18	17	7	1.43	R	[32]	[33]
SN 2004dj	SN, Type IIP	2004 Aug 05	2004 Nov 24	110	11	5.0	V	[34]	[35]
SN 2004dk	SN, Type Ib	2004 Aug 07	2004 Sept 18	41	5	8.5	R	[36]	[37]
SN 2004et	SN, Type II	2004 Oct 07	$2004 \ \mathrm{Dec} \ 03$	57	9	5.0	R	[38]	[39]
SN 2004gq	SN, Type Ib	$2004~{\rm Dec}~08$	2005 Jan 21	35	5	8.5	R	[36]	[37]
SN 2007bg	SN, Type Ic	2007 Apr 30	2007 Jul 24	68	6	8.46	R	[40]	[41]
SN 2007gr	SN, Type Ic	2007 Aug 17	2007 Nov 18	92	8	4.9	R	[42]	[43]
SN 2007uy	SN, Type Ib	2008 Jan 11	2008 Mar 07	56	12	8.4	R	[44]	[44]
SN 2008D	SN, Type Ib	$2008~\mathrm{Jan}~15$	2008 May 10	115	7	4.8	R	[45]	[46]
SN 2008ax	SN, Type IIb	$2009~\mathrm{Mar}~07$	2008 Apr 21	46	9	8.46	V	[47]	[47]
SN 2009bb	SN, Type Ic	$2009~\mathrm{Apr}~05$	$2009~\mathrm{May}~20$	44	10	8.46	V	[48]	[49]
GRB 970508	GRB	1997 May 15	1997 Aug 04	82	11	8.46	R	[50]	[51]
GRB 991208	GRB	$1999~{\rm Dec}~10$	$2000~\mathrm{Jan}~17$	37	7	8.46	R	[52]	[53]
GRB $000301C$	GRB	$2000~{\rm Mar}~05$	2000 Apr 18	43	6	8.46	R	[54]	[55]
GRB 030329	GRB	$2003~\mathrm{Mar}~30$	2003 June 04	65	20	8.64	R	[56]	[57]
GRB $050820A$	GRB	$2005~\mathrm{Aug}~20$	$2005 \text{ Sept } 15/26^*$	25	6	8.46	R	[58]	[58]
GRB 060218	GRB	2006 Feb 20	2006 Mar 15	23	12	8.46	R	[59]	[60]
GRB 070125	GRB	$2007~\mathrm{Jan}~31$	$2007~{\rm Feb}~18$	18	6	8.46	R	[61]	[61]
GRB 100418A	GRB	$2010~\mathrm{Apr}~20$	$2010~\mathrm{May}~21$	31	7	8.46	$white\ filter$	[62]	[63]
BL Lacertae	Quasar	1994 June 28	2005 Jan 12	3851	265	5.0	R	[64]	[64]
3C 454.3	Quasar	2008 May 08	2010 Jan 28	630	79	8.0	R	[65]	[65]

^{*} In the case of GRB 050820A the last pair of F_0 and F_T measurements were separated by 11 d.

which had long-term (ideally ≥ 1 month) well sampled light-curves. Simultaneous measurements were still important although we relaxed the time required between measurements to 3 d in order to achieve a good sample size with well sampled light-curves. The sample, of which details can be found in Table 2, contains 5 transient/flare CV events, 8 XRB

transient/flare events, 15 SNe, 8 GRBs and 2 quasars for a total of 38 dynamic sources. As our quasar sample did not allow for individual light-curves, two quasar objects with good coverage were specifically found to include. One of the quasars is BL Lacerate which we consider a 'quasar' for our purpose (as we did with the radio selected quasars). The cov-

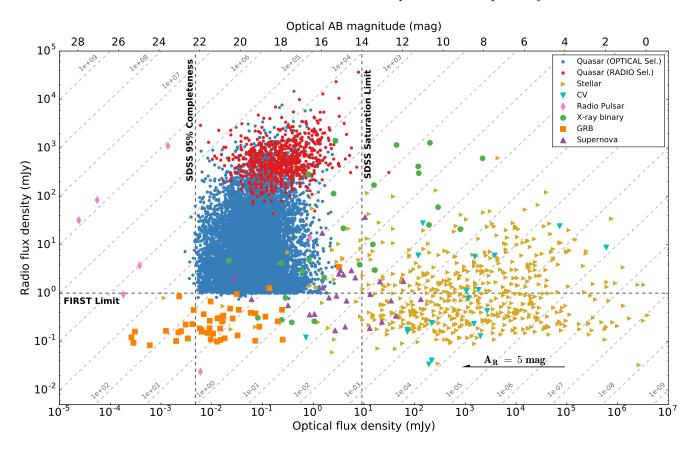


Figure 1. F_0 versus F_r of our sample of objects from different classes. The F_0 values have been converted from mag to mJy, with the optical magnitude scale given as a reference on the top axis (based upon the R band). The data contains F_0 in bands V and R and the F_r covers a range of frequencies from 1–10 GHz. Labelled on the plot are: a horizontal line denoting the FIRST survey source detection threshold (1 mJy); a vertical line denoting the SDSS 95 per cent completeness limit (~22 mag), and another showing the SDSS saturation limit (14 mag). The diagonal lines in the background of the plot show the lines of constant ratio between the two flux density values corresponding to changing distance and are labelled with respective ratio. A 5 mag scale arrow is also shown to show the possible effect of extinction on the optical magnitudes. Please refer to the online print for a colour version of the figure.

erage of these events range from 2 weeks to 10.5 yr. The only exception of the 3 d pair requirement is the last measurement of GRB 050820A, which were recorded 11 d apart due to lack of simultaneous coverage. Also, three sources have the F_0 recorded in 'Visible' (V1500 Cyg and V1974 Cyg; both CVs) or 'white filter' (GRB 100418A) as these were the only optical bands available and were judged to be suitable for the dynamic purpose.

The 'state' of the CVs and XRBs in the dynamic sample is not as trivial as for the SNe and GRBs, hence the details of the circumstances of these sources can be found in Tables A2 and A3. In summary, the five CVs are measurements of outbursts where the first simultaneous measurements occur between 1.3–66 d after the optical maximum or outburst itself. For the XRBs, seven are simultaneous measurements beginning between 3–14 d following the detection of an outburst at X-ray wavelengths. The exception is GX-339 where the measurements monitor the decline of a flare that occurred approximately 1 yr prior. During the decline the source undergoes a small re-flaring in both $F_{\rm r}$ and $F_{\rm o}$ as it transitions from the soft to hard state.

The radio frequencies and optical bands used have been kept as consistent as possible over the dynamic data. In addition, within the coverage of each source the entire lightcurve is in one single radio/optical frequency/band only. We note that such long coverage of objects may signify a unique characteristic of the event. For example, SN 1993J and GRB 030329 represent some of the brightest radio events of their classes. Thus, while these sources offer a good example of how classes are likely to evolve, they are not fully representative.

3 RESULTS

We attempted various methods to visualise the dataset detailed in Section 2 to find a scheme which offered the best separation between classes. This included using parameters such as the ratio of flux density values, i.e. $F_{\rm r}/F_{\rm o}$, and optical colours. We found that plotting $F_{\rm o}$ against $F_{\rm r}$, in log space, is the most useful diagram in terms of being able to distinguish the different classes. Further reasoning behind this choice is discussed in Section 4. The result is presented in Fig. 1.

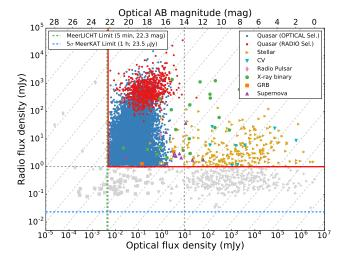


Figure 2. Denoted by solid red lines is the boundary for which our sample is the most 'complete', i.e. those sources (plotted in colour) which are brighter than a R magnitude of 22 in the optical (the SDSS 95% completeness) and 1 mJy in the radio (the sensitivity limit of the FIRST survey). Also plotted are the limits that define the region that will be explored by the MeerKAT and MeerLICHT telescopes in the radio and optical respectively.

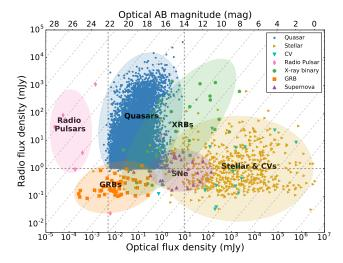


Figure 3. A simplistic schematic version of the base result where coloured ellipses represent the space where the majority of different classes of objects occupy in the plot.

3.1 Description of the base result

The plot shown in Fig. 1 provides an overview of where each class of object, given our data and its limitations, typically lies in the F_r - F_0 parameter space. We have converted the optical magnitudes to millijansky units in order to make a direct comparison to the F_r measurements (an optical magnitude axis is provided at the top of the figure for reference). This was done using the zero flux point of 3631 Jy as we had converted all magnitudes, where appropriate, to the AB system.

A series of lines are also displayed on the plot. First, there are background diagonal dashed-lines that represent

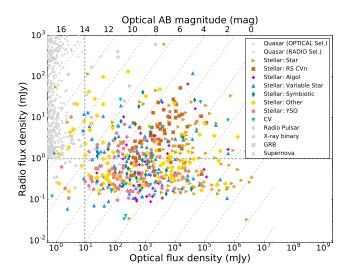


Figure 4. The stellar sample plotted sub-categorised along with CVs on a 'greyed out' version of the main plot. It shows that there is no clear trend to be able to use the stellar sub-classifications.

the slope of a constant F_r and F_0 ratio (the ratio values are also labelled on the plot for each line). This means that if a particular source was moved closer to Earth, or further away, it would move on the plot along this gradient. Second, the arrow in the lower right-hand section of the plot demonstrates the movement an object could undergo with a reddening equal to 5 mag. Third, and most importantly, there are lines signifying the flux density limits of the surveys used to gather the optically selected quasars, which has a large influence on the result. The horizontal line indicates the 1 mJy source detection threshold of the FIRST survey. The two vertical lines denote the SDSS saturation limit (14 mag, R band) and the SDSS 95 per cent completeness limit (22 mag, R band). As can been seen in Fig. 1, the limits greatly impact the ability to separate classes, especially in the case of the quasars where the abrupt 1 mJy limit of the FIRST survey artificially isolates the GRBs. The reliance on the FIRST survey makes this unavoidable and we specifically address this problem in Section 4.1.

Considering the limits, Fig. 2 signifies the region of the plot that is considered the most complete area of the sample, i.e. the area contained by the limits of FIRST and SDSS which are shown by solid red lines, along with sources in the 'complete area' being presented in colour. Also on Fig. 2 we have shown estimates of the region that will be explored by MeerKAT and MeerLICHT, assuming a 1 h, 5σ MeerKAT sensitivity of 23.5 µJy (Taylor & Jarvis 2017) and a 5 min optical depth of 22.3 mag (r-band) for MeerLICHT (Bloemen et al. 2016). Fig. 3 presents a schematic version of the full area of the plot in Fig. 1, to further illustrate the areas of certain classes. It is created by placing ellipses centred on the median points of the respective populations data and then manually sized to enclose the majority of the populations. As such, Fig. 3 is primarily meant as a visual demonstration, and is presented with the same caviet as discussed above in that the quasars would extend into the GRBs with a more complete sample.

From Figs. 1–3, we see that there is a good separation between Galactic and extragalactic populations in our

dataset both in the 'complete' and overall regions. On the right half of the plot reside the stellar and CV populations, while classes such as quasars and GRBs typically reside on the left hand side. SNe are mostly placed between these two Galactic and extragalactic populations. The same is true of the XRBs however they are much more chaotic and span a large region that reaches the extragalactic area, highlighting the very dynamic nature of these objects. The Galactic/extragalactic separation is likely due to the detected radio stellar objects in our sample being relatively nearby (hence their detection), therefore they appear bright in the optical. Note that we do not attempt to further sub-classify the stellar sources, using the information from the dataset (see Section 2.3). As shown in Fig. 4, the subclasses of the stellar sample did not offer any distinct separation, hence we remained with the global 'stellar' definition. Fainter in F_0 are the GRBs which are currently well separated from the rest of the classes due to the FIRST 1 mJy limit as previously discussed (we attempt to address this in Section 4.1), although the GRBs themselves are relatively clustered together. As for the quasars, there is no distinction between the optically and radio selected samples, with the radio sample occupying the radio-bright section of the former. Hence, from here on we group the two samples under one class of 'quasars'. Lastly, the majority of the radio pulsar population are positioned to the far left-hand side of the plot due to their faint F_0 . The faintness of the radio pulsars in F_0 means that they are not contaminated by other classes in our current dataset, although again, this is largely due to SDSS optical limit. We note that the discussed distinctions are primarily due to the F_0 , though this was our original aim. The F_r becomes important once we consider sources beyond our current limits (Section 4.1).

3.2 Dynamic characteristics

The results of the dynamic data have been split over two figures: the upper panel of Fig. 5 shows paths which are traced out by the 38 objects, grouped by class, of the dynamic data sample (detailed in Section 2.8 and Table 2), overlaid on a 'greyed-out' version of Fig. 1. The lower panel of Fig. 5 shows only the 'start' and 'end' points of the tracks with respective labels linking the data points of an individual source. The nature of the sample means that the 'start' and 'end' refer to different points in the time line of the event respective to one another. Hence, for a more detailed view, the individual tracks from each class of object (with the exception of the quasars) are shown in Fig. 6. In this figure, the tracks are labelled with the number of days that have elapsed since the first observation in the case of CVs and XRBs, or the number of days after the explosion date for SNe and GRBs (the non-standardised reporting of 'day 0' for XRBs and CVs is the reason for the difference). A reminder that the timespan of the objects range from ~2 weeks to 2 yr (with the exception of BL Lacerate which covers 10 yr) and that each track uses only a single frequency or optical filter. Overall, from Fig. 5 the majority of classes appear to evolve within the static areas as discussed in the previous section (Fig. 1 and 3). This can largely be seen by looking at the 'start' and 'end' points in the lower panel of Fig 5. The exception to this is the SNe which brighten in the radio considerably during their evolution. The XRBs also still have a large overlap with other classes, especially SNe. Below we expand on the features of each class.

3.2.1 Accreting sources

Starting with the two quasars, for which 3C 454.3 is the source brighter in the radio with BL Lacertae below, it can be seen that these move very little over time in $F_{\rm r}$ relative to the other classes presented in the figure. In both cases, the two quasar objects do not show large relative flux density variation events like those seen in other classes, in addition to varying back and forth rather than following a clear track. 3C 454.3 is monitored for 630 d which is similar order of magnitude to the timespan covered by three CVs and one SN, which show much more variation over the same timescale. As the quasars are quite static on the plot they are not displayed in Fig. 6.

The CVs appear quite uniform in their dynamic characteristics. Initially detected as bright optical objects, the brightest in the dynamic sample, they proceed to decrease in F_0 while the F_r rises and falls again. The sources follow a simple model in which the optical flare evolves more rapidly than the radio resulting in an 'anti-clockwise loop' appearance of the track. This is a characteristic that is shared with other classes on the plot such as GRBs and SN. Hence, anticlockwise loops are a common occurrence. The 'start' of the measurements in the sample occurs 1-2 months after the optical detection, i.e. when the first radio detections were made, and therefore the optical is seen to decline. The exception to this is SS Cyg, the dwarf nova, that was observed in radio rapidly (1.3 d) after the detection of an optical flare. The radio flare from SS Cyg also rose and faded quickly as seen by its track.

The tracks of the XRBs are less uniform and reflect the overall sample characteristic of appearing at a diverse range of areas on the plot, both in start and end points. As stated in Section 2.8, most of the sources are observed in a declining state after the detection of an X-ray flare, and a rapid decline in both F_r and F_o is what is most commonly seen on the plot. Although the F_0 of GS 1124-684 remains steady during the radio decay and experiences a re-flaring in the radio. A rise in F_r is detected in three sources: GRO J1655-40, GX 339-4 and XTE 1859+226. GX 339-4 after the radio rise mimics the steady decline of the other sources, however the other two sources show more complex behaviour. GRO J1655-40 continues to rise in F_0 while the F_r , rises, peaks and decays all during this period, hence why it is the only XRB to end brighter in F_0 in the sample. XTE 1859+226 on the other hand experiences many smaller radio flares during the optical decay, hence its erratic appearance, though it should be noted that this is data from the Green Bank Interferometer (GBI) database and therefore the sampling of the radio light-curve is very frequent compared to other sources (the source contains 42 pairs of measurements over 2 months compared to 16 for the next most sampled source).

3.2.2 Explosive events

SN would be expected to follow the anti-clockwise motion as discussed with the CVs, and two SN show a very good example of that, 1993J (type II) and 1994I (Ic). They both rise steadily in the radio band, with only a slight increase,

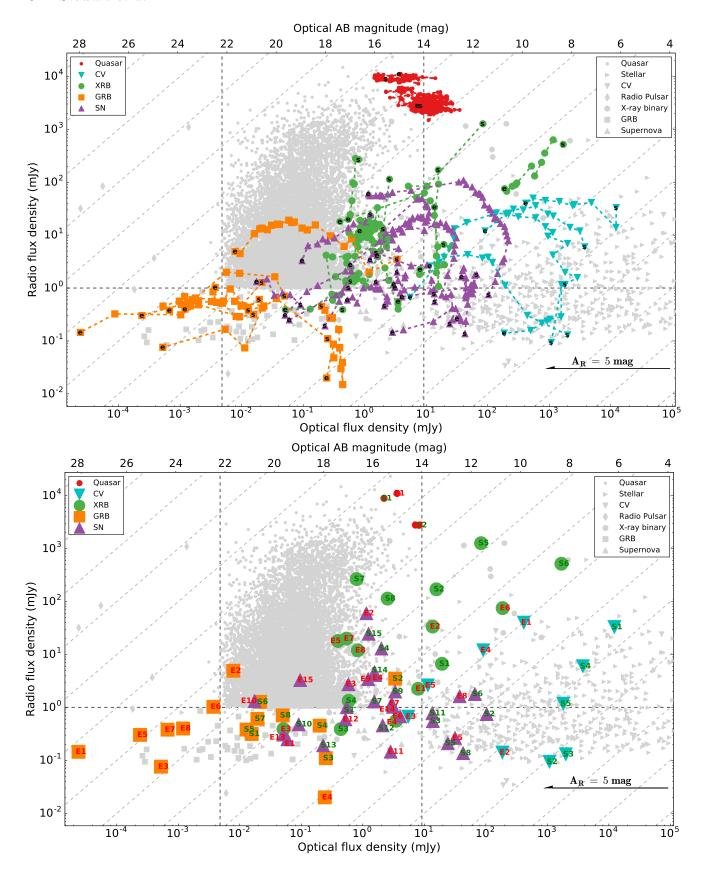


Figure 5. Upper panel: Plotted are the 'tracks' for which the dynamic sources follow as the astrophysical events evolve over time. Due to the number of sources they are plotted in groups of the respective class of which there are two quasars, five CVs, eight XRBs, 15 SNe and eight GRBs (refer to Table 2 for details of the objects). These are plotted over a 'greyed-out' version of the basis diagram to allow comparison. The start and end of each track are labelled with 's' and 'e', respectively. Lower panel: In this figure only the start and end points of the tracks are plotted for clarity, with each point labelled with a green 'S' or red 'E' for the start and end point, respectively, points of the tracks are plotted for clarity, with each point labelled with a corresponding number to pair them. Please refer to the online print for a colour version of the figure.

MNRAS in press, 1–21 (2018)

Figure 6. The tracks of individual sources in the dynamic sample plotted per class. The start and end of each track is denoted by a green and red ring around the data point, respectively. Also on every start, end and every third data point (this frequency varies due to avoid congestion on the plot) is the number of days that has passed. For CVs and XRBs the day 0 refers to the first observations, however for GRBs and SNe it refers to the explosion date. Upper left: XRBs, upper right: CVs, lower left: SNe and lower right: GRBs. Please refer to the online print for a colour version of the figure

Optical flux density (mJy)

Optical flux density (mJy)

1

and then decrease, in the optical band. The reverse scenario then becomes true for the later part of the tracks where the $F_{\rm r}$ changes slower than the now decreasing $F_{\rm o}$. Generally, SNe follow this trend, and from the first pair of measurements, the track will tend to proceed in the upper-right direction, i.e. brighter in F_r and F_0 before looping around in the anti-clockwise motion. However, there are some SNe that behave differently. For example, SN 1998bw (Ic) moves instead in a tight clockwise motion. This is due to SN 1998bw experiencing a rapid rise to its peak $F_{\rm r}$ (~10 d), compared to, for example, SN 1994I (\sim 20 d) as seen in Fig. 6. SN 2009bb, another type Ic, also shows a steady decline after 12 days, suggesting a similar event to that of SN 1998bw. SN 2007bg (Ic) is unique in that it appears very near the GRB region and also initially mimics the track 'shape' of other GRB sources. A year after discovery, persistent strong radio emission detected by Prieto, Watson & Stanek (2009) suggested that SN 2007bg could be a good candidate for an off-axis GRB. Although this was later deemed unlikely with further analysis by Salas et al. (2013), the plot could prompt this suggestion from the track shape and placement.

The GRBs also follow an anti-clockwise motion, though with a much more muted rise in F_r than seen in SNe, and also are mainly all contained within the previously defined GRB area of the plot. Two sources stand out: GRB 030329, which appears to be very bright in the radio, and GRB 060218 that does not follow the common GRB track trajectory of a slowly decaying radio source. Instead it decays in the radio very swiftly. First, GRB 030329 was a nearby afterglow (z = 0.1685, 587 Mpc; Greiner et al. 2003) and at the time was the brightest GRB afterglow in the radio ever observed. Thus, its position on the plot is boosted in F_r such that it transits the quasar area. If the GRB was moved further away, e.g. the same as GRB 100418A (z = 0.624, 1.4 Gpc; Antonelli et al. 2010), the 10 mJy flux density becomes ~1 mJy - consistent with the other GRBs in the sample. Due to its brightness and well sampled light-curve. the anti-clockwise nature of the track can be clearly seen. GRB 060218 on the other hand is defined as an X-ray flash (XRF), and had unique properties in that it was relatively nearby $(z = 0.0335, \sim 145 \text{ Mpc})$ and the burst itself lasted a long time ($\Delta t \approx 2,000 \text{ s}$). Indeed, Soderberg et al. (2006a) showed that the event was a hundred times less energetic but ten times more common than cosmological GRBs.

The dynamic data sample has shown how taking into account how a discovered object evolves over time - considering the time scale of change and the positioning - could potentially aid the ability to separate classes where confusion occurs. This is discussed further in the following sections.

4 DISCUSSION

We have presented a representation of the $F_{\rm r}$ and $F_{\rm o}$ measurements for a wide range of transient and variable sources, showing that it is possible that this information alone can differentiate between Galactic and extragalactic populations. Here we give more detailed discussion of the obtained results.

First, given how the data is presented in Fig. 1, we believe the range of radio frequencies does not have a negative impact. For example, assuming a canonical spectral index

of $\alpha = -0.8$ (for optically thin synchrotron emitting sources; Kellermann 1966), a 1 Jy source at 1 GHz becomes ~0.2 Jy at 10 GHz, a one order of magnitude change. A difference of two orders of magnitude would mean $\alpha = -2.0$. Hence, given the populations we are sampling (likely $\alpha \sim -0.8$), a spread of one order of magnitude does not impact our ability to differentiate classes. We also note that we have not considered measurement uncertainties when compiling our results. We believe that because of the nature of what we are investigating, the intrinsic spread of each population in the F_r - F_0 parameter space has a much greater influence than that of measurement error. We also acknowledge that the dataset created in this investigation is a biased sample, due to the many different sources used to build it. At this initial stage of the project, we do not attempt to un-bias the data due to the complexity of the task. Though, we acknowledge that correcting for the biases is an important future step in constructing more detailed models from the dataset. Lastly, we have not corrected our optical sample for extinction. If this was accounted for, it would cause sources to shift left along the x-axis only, as denoted by the red arrow on Fig. 1. We did not wish to 'de-redden' our sample as we wanted to probe measurements that are directly observed, such that the dataset could potentially be used as soon as observations are recorded.

As for the different parameters considered discussed earlier in Section 3 - we first considered using the ratio of F_r/F_0 and plotting this against F_r . As can be interpreted from our final choice, this ratio value also allowed us to somewhat separate classes, especially in the case of Galactic or extragalactic objects. Fig. 7 shows the distribution of F_r/F_0 for each class of object. However, this representation did not offer any advantages over plotting the F_r and F_o against each other and hence was not used in the final plot. Another parameter that was tested was optical colour, which we had originally attempted to obtain, although the total percentage of the sample for which colour was obtained varied largely per class (99 per cent of the quasar sample, 75 per cent of the SNe, 40 per cent of CVs, 25 per cent of the GRBs and 20 per cent of the XRBs). We found that plotting optical colour versus $F_{\rm r}$, or versus the ratio of $F_{\rm r}/F_{\rm o}$, greatly hindered our ability to separate different classes of objects. This was primarily caused by the narrow range of optical colour values, which limited the parameter space in which the classes could be separated. For example, with this parameter we could no longer distinguish Galactic and extragalactic populations. Hence, due to this and the limited available data we did not pursue optical colour any further at this time.

4.1 Extending the sample beyond the current limitations

As discussed previously, the location of quasars on the plot is currently not a complete representation and greatly impacts the ability to identify areas where classes are separated. This is due to the sensitivity limits of the surveys we have used to build our sample, in particular, the SDSS 95 per cent completeness limit of ~ 22 mag, and the FIRST source detection threshold of 1 mJy (refer to Section 2.2). The populations would exceed these limits when observed with improved sensitivities, and therefore extend into areas where other classes are present - causing confusion. A similar notion could be

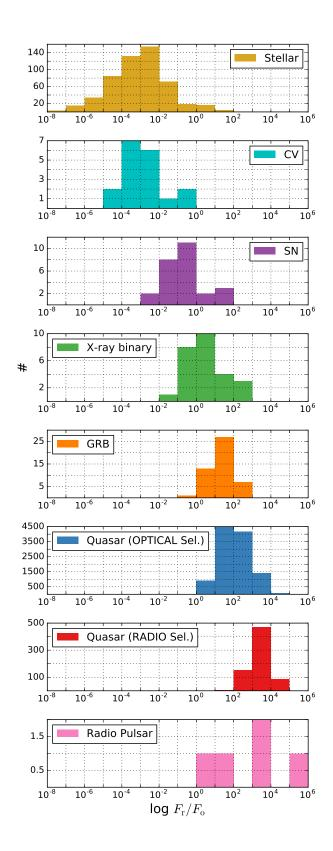


Figure 7. The distribution of the ratio F_r/F_0 for each class included in the sample.

applied to the stellar sample, as this will be another general class of a large size that will continue to be detected as observations probe deeper.

Extending the quasar sample with telescope data is currently challenging given the lack of wide-field radio surveys that probe deeper than the FIRST limit. One of the larger surveys that has probed deeper is a survey of the SDSS 'Stripe 82' area of sky at high-resolution using the VLA at 1.4 GHz done by Hodge et al. (2011). The survey covers 92 deg^2 with a median rms noise of 52 μ Jy beam⁻¹. The SDSS Stripe 82 survey consists of 275 deg² of sky that was visited multiple times by the SDSS camera, and hence reaches ~ 2 mag deeper than the areas with single visits (Annis et al. 2014). As part of the radio survey, Hodge et al. (2011) discovered 76 new radio quasars by cross matching with the SDSS data. The left panel of Fig. 8 shows the discovered faint quasars added to our plot, where it can be seen that the sources appear directly below our quasar sample, where previously the GRBs were isolated.

While the Stripe 82 quasars begin to show how the quasars will extend, we can further demonstrate the effect of deeper sensitivities by showing how the current sample would appear if the distance from Earth was increased. The optically selected SDSS quasars are shifted such that the flux density measurements are approximately 10 and 100 times fainter (moved in distance by a factor of $\sqrt{10}$ and 10 respectively). As the redshifts for the quasars are known from SDSS, we were also able to apply a K-correction and correct for bandwidth stretching. The luminosity with the corrections applied is

$$L = 4\pi F d_{\rm L}^2 (1+z)^{-\alpha-1},\tag{1}$$

where L is the luminosity, F is the flux density, $d_{\rm L}$ is the luminosity distance, z is the redshift and α is the power-law spectrum index. For the radio we use the previously defined canonical value of $\alpha_{\rm r}=-0.8$ and the for the optical a value of $\alpha_{\rm o}=-0.44$ (Vanden Berk et al. 2001). For the stellar population, our sample includes parallax distance measurements for 451 of the 534 stellar objects plotted, for which the median value is 142 pc. Thus, we use this information to increase the distance of these stellar objects by 1 kpc. The results of these shifts can be seen in the right panel of Fig. 8.

The extension of the quasars completely covers the area of the plot that was previously only occupied by GRBs, along with approaching the pulsar region. This suggests that when observing beyond the limits of our current sample, it will prove difficult to differentiate a GRB from a quasar with a single pair of measurements. The stellar sources extend down to an F_r of 1 μ Jy, with some sources going beyond this value. The region below the stellar sources on the basis plot was empty, hence, unlike the quasars, the extension of the stellar sources does not cause confusion with other sources. It is worth noting that the distinction between quasars and stellar sources, i.e. Galactic and extragalactic objects, remains relatively clear. However, the F_r becomes much more relevant when determining the Galactic-extragalactic boundary. The extended stellar sources have similar F_0 to that of the original quasar sample, hence the F_r becomes a useful differentiator between the classes.

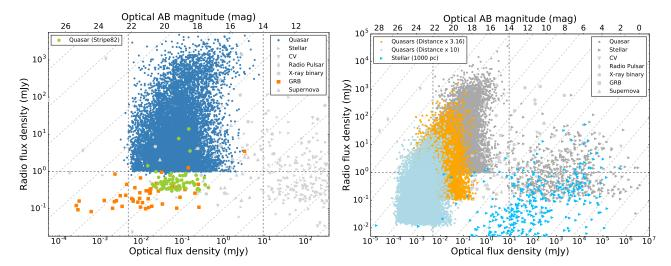


Figure 8. Left: The faint quasars of the VLA Stripe 82 survey have been added to the plot where the other sources have been 'greyed out' with the exception of the sample quasars and the GRBs. It shows how the fainter quasars overlap with the previously isolated GRBs. Right: The effect of probing the quasar and stellar populations to a deeper sensitivity, by increasing the distance of those sources contained in the sample. This is overplotted on a 'greyed-out' version of the basis plot with the original quasar and stellar sources highlighted by a darker shade. Please refer to the online print for a colour version of the figure.

4.2 Transient diagnostic application

To help demonstrate the use of the current dataset to provide an initial class approximation of radio sources, we perform a small scale blind test using a catalogue of variable and transient radio sources discovered in the FIRST survey, as compiled by Thyagarajan et al. (2011) (hereafter the 'T11 sample'). We impose the following criteria on the sources we select from the catalogue:

- (i) sources must have a defined SDSS *i*-band magnitude, which are mostly gathered by the authors from the SDSS DR7 catalogue. SDSS-*r* band would be more ideal but for the purposes of the test, plus to keep within the already done cross matching, the SDSS-*i* is adequate enough for our use.
- (ii) only sources which are not flagged as being in the vicinity of another source brighter than 500 mJy.

The authors also attempted to classify the candidates by cross-matching with a variety of catalogues and databases. The sources are labelled as either transient or variable. For the test we select the candidates that have the classifications as defined by the authors of:

 ${\bf SDSS}\text{-*}$ - an unclassified SDSS counterpart (transient and variable).

SDSS-QPO (S) and (P) - quasars from the SDSS spectroscopic (S; Schneider et al. 2007) and photometric (P; Richards et al. 2009) quasar catalogues (only contain variables).

SDSS-GAL - objects classified as galaxies in SDSS (select transients only).

Tycho-Star - counterpart found in the Tycho star catalogue (Høg et al. 2000, only contain variables).

HIP-Star - counterpart found in the Hipparcos star catalogue (Perryman et al. 1997, only contain variables).

We do not consider SDSS-Gal variables due to these sources effectively being already classified, in addition to our previ-

Table 3. The total number of each type of object included in the test sample.

Object Type	Total No.
Unclassified (Variable)	89
SDSS-QSO (Variable)	100
Star (Variable)	3
SDSS-Gal (Transient)	5
Unclassified (Transient)	1
Total	198

ously stated desire to focus on optically point-like transient or variable objects. However, it should be noted that radio transients may appear coincident with extended optical objects, but can be difficult to associate the two unambiguously. Hence, this scenario would not be ignored in a blind search. For the purposes of our test we define our own categories of:

Unclassified (Variable) (SDSS-* variables). SDSS-QSO (Variable) (SDSS-QPO S,P variables). Star (Variable) (Tycho/HIP-Stars, variables). SDSS-Gal (Transient). Unclassified (Transient) (SDSS-* transients).

In total we include 198 objects in our testing sample, the by-category totals can be found in Table 3. We plot the F_{Γ} and F_{0} values of the 198 transient and variable objects onto the basis diagram, for which the result is shown in Fig. 9.

We see an agreement with the classified 'Star' and 'QSO' objects, in that they lie within the stellar and quasar regions respectively, a distinction that could have been possible without the prior classifications. This is the immediate first advantage of the basic method - the separation between Galactic and extragalactic objects - at least in the sample we currently have available. It is a promising first step of using such a photometric method to provide a swift classification,

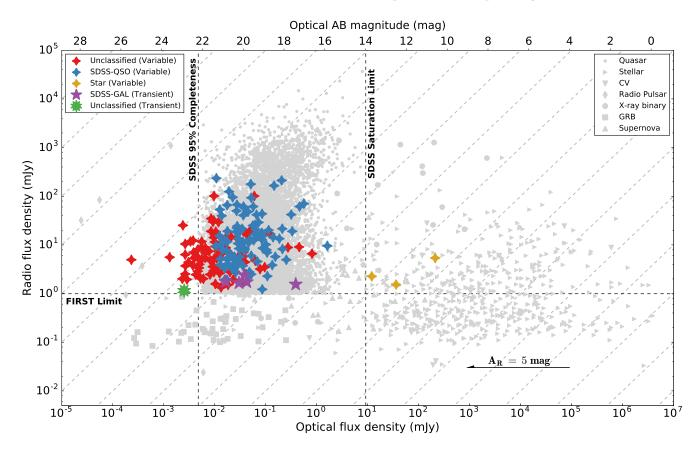


Figure 9. The result of plotting the selected radio transients and variables from the FIRST survey (Thyagarajan et al. 2011), categorised by their highest ranked counterpart at other wavelengths deduced by the authors of the catalogue, upon a 'greyed-out' version of the basis plot. Please refer to the online print for a colour version of the figure.

and also a useful property. In a scenario with a high yield of transient sources, the basic distinction could be used to direct further follow-up. Although, classifying deeper than this is challenging, and in the current form of the method, attributing a definitive class is not possible. Without the prior classifications from the T11 sample, it would be difficult to firmly identify an object that might not belong to the quasar population. Though, it should be noted that the majority of these sources are likely to be quasars, and are classified as such by both methods. One exception is the optically very faint 'Unclassified variable' that is noticeably separate from the main quasar cloud near the pulsar region. but even so, it is again more than likely to be part of a optical faint quasar population. Given the current data, this would be an example of a source to be initially followed up. If the T11 sample was not using the FIRST survey then we may have seen some objects below 1 mJy, making such objects more likely to belong to the GRB population. Unlike the sub-stellar populations, it may be that the extragalactic areas of the plot have areas of a specific class, such as GRBs or SN, which do seem to be grouped, despite the inevitable extension of the quasar population (Section 4.1).

4.3 Future steps

Building a probability model using the dataset is the natural progression of this work, and would continue to see advancement and refinement with the addition of further data over time. Accounting for the bias of the extremely diverse dataset is, again, important for this step, but complex. Though, in its current form, we believe the dataset already offers usefulness in gaining an initial diagnostic.

Combining this method with other techniques and external knowledge can only enhance its accuracy. We previously showed how a sample of sources evolve on the plot over time (Section 3.2). A more thorough analysis of this feature may unveil trends unique to certain classes that could be recognised by an algorithm within the F_r and F_0 parameter space, meaning that new sources could be classified with a high probability and minimal monitoring time (though the 'minimal monitoring time' would also need to be established). This would also open up cross examining the rise/decline times of the events in question with existing classification techniques both the radio (Pietka et al. 2015, 2017) and optical (Kasliwal 2011). Knowledge such as whether the optical counterpart is an extended object, or if the object was present in historical catalogues is also simple information that offer clues as to the associated class. In time, the addition of a third parameter (e.g. X-ray flux density) could also be achieved.

We stress and remind that we are assuming an era where the rate of detected radio transients and variables is much greater than it is at present. Obtaining a spectrum of a counterpart will usually provide the most definitive clue of an objects associated class. Though with potentially hundreds or thousands of candidates, a spectra may not be feasible to obtain swiftly in order to be fed into ongoing observation strategies with specific science goals. The presented $F_r - F_0$ method is purposely simple for it is an initial analysis of what can be achieved with current $F_r - F_0$ data. The simple test performed above shows that it is difficult to obtain precise classifications outside of being Galactic or extragalactic. But, advancing the $F_r - F_0$ dataset itself, along with combining the method with other information and techniques, can provide an important initial diagnostic method in a future classification system.

5 CONCLUSIONS

We have presented an initial study of the optical counterparts to a wide range of radio transients and variables, with the eventual aim of using such a dataset to help classify a blindly detected radio event. We collected a sample consisting of 12,441 pairs of $F_{\rm r}$ and $F_{\rm o}$ measurements from seven classes of astrophysical objects, including populations such as quasars, GRBs, CVs and SNe. These measurements were recorded by numerous radio and optical facilities, at frequencies ranging from 1–10 GHz and optical filters V and R. The dataset has a significant bias due to the diverse range of classes of object and sources of information. However, our approach at this stage was to provide an early assessment, meaning that we do not yet tackle the complex biases.

We found that comparing the $F_{\rm r}$ and $F_{\rm o}$ measurements of each object provided a useful separation between Galactic and extragalactic sources. Radio emitting stars and CVs, for example, are distinctly in a different area to that of quasars and GRBs. However, differentiating between distinct individual classes with a high accuracy is challenging. Types of stellar sources were found to be impossible to separate, but pulsars and extragalactic sources such as GRBs were found to be isolated. Although, the isolation is caused by the limitations of our sample, specifically the detection limit of the FIRST survey used for quasars. Fainter radio quasars beyond this limit will lead to confusion with previously isolated classes. We also investigated how a sample of 5 transient/flare CV events, 8 XRB transient/flare events, 15 SNe, 8 GRBs and 2 quasars evolved in the parameter space over time - a possible unique feature that could be used to provide more accurate classifications with minimal monitoring. We showed that CVs, SNe and GRBs follow similar 'tracks' in the parameter space, in that they generally follow an 'anticlockwise' loop on the plot - a motion that would be repeated for any class that follows a model of the optical flare evolving more rapidly than the radio. XRBs on the other hand are quite varied in nature where as quasars tend to move relatively little over the same time frame. Lastly we used a sample of radio transients and variables identified in the FIRST survey to highlight the features discussed above.

The next step of our investigation will be to use our dataset to provide a probability of an object belonging to a class, for which it is also important to understand the biases. Though in its current form, the dataset can already provide a useful first estimate of a discovered source, albeit crude. However, once used alongside other classification techniques and information it is likely to help provide accurate predic-

tions. In addition, the method can also be iterated on and improved as further simultaneous multi-wavelength data is recorded. For example, the MeerLICHT project, which will provide simultaneous optical data to MeerKAT radio observations, is a unique opportunity for a detailed dataset in the near future. A need for a classification system assumes an era in the future where a high number of radio transients and variables are regularly being blindly detected. Ideally these systems would be automatic, likely using machine learning techniques and subsequently able to make appropriate decisions on further follow-ups depending on the science goals.

ACKNOWLEDGEMENTS

We thank the anonymous referee for their detailed comments that helped to improve our analysis and presentation. We acknowledge support from the European Research Council via Advanced Investigator Grant no. 267697 4 Pi sky: Extreme Astrophysics with Revolutionary Radio Telescopes (PI: R.P. Fender). T.M.-D. also acknowledges support via a Ramón y Cajal Fellowship (RYC-2015-18148) and the the Spanish MINECO grant AYA2017-83216-P.

The authors wish to thank Manuel Güdel for providing us with the formatted data on the flux density characteristics of the stellar sources.

This research has made use of data taken and assembled by the WEBT collaboration and stored in the WEBT archive at the Osservatorio Astrofisico di Torino - INAF (http://www.oato.inaf.it/blazars/webt/). We thank Claudia Raiteri and Massimo Villata for supplying the WEBT AGN monitoring data.

The authors also wish to thank Deanne Coppejans for providing extra information on the CVs used in the sample.

We acknowledge with thanks the variable star observations from the AAVSO International Database contributed by observers worldwide and used in this research.

This paper has made use of up-to-date SMARTS optical/near-infrared light-curves that are available at www.astro.yale.edu/smarts/xrb/home.php. The Yale SMARTS XRB team is supported by NSF grants 0407063 and 070707 to Charles Bailyn.

This research has made use of the SIMBAD database and the VizieR catalogue access tool, operated at CDS, Strasbourg, France.

The Green Bank Interferometer is a facility of the National Science foundation operated by NRAO with support from the NASA High Energy Astrophysics program.

Funding for the SDSS and SDSS-II has been provided by the Alfred P. Sloan Foundation, the Participating Institutions, the National Science Foundation, the U.S. Department of Energy, the National Aeronautics and Space Administration, the Japanese Monbukagakusho, the Max Planck Society, and the Higher Education Funding Council for England. The SDSS Web Site is http://www.sdss.org/.

The SDSS is managed by the Astrophysical Research Consortium for the Participating Institutions. The Participating Institutions are the American Museum of Natural History, Astrophysical Institute Potsdam, University of Basel, University of Cambridge, Case Western Reserve University, University of Chicago, Drexel University, Fermilab, the Institute for Advanced Study, the Japan Participation

Bloom J. S., et al., 1998, ApJ, 508, L21

Group, Johns Hopkins University, the Joint Institute for Nuclear Astrophysics, the Kavli Institute for Particle Astrophysics and Cosmology, the Korean Scientist Group, the Chinese Academy of Sciences (LAMOST), Los Alamos National Laboratory, the Max-Planck-Institute for Astronomy (MPIA), the Max-Planck-Institute for Astrophysics (MPA), New Mexico State University, Ohio State University, University of Pittsburgh, University of Portsmouth, Princeton University, the United States Naval Observatory, and the University of Washington.

Funding for SDSS-III has been provided by the Alfred P. Sloan Foundation, the Participating Institutions, the National Science Foundation, and the U.S. Department of Energy Office of Science. The SDSS-III web site is http://www.sdss3.org/.

SDSS-III is managed by the Astrophysical Research Consortium for the Participating Institutions of the SDSS-III Collaboration including the University of Arizona, the Brazilian Participation Group, Brookhaven National Laboratory, Carnegie Mellon University, University of Florida, the French Participation Group, the German Participation Group, Harvard University, the Instituto de Astrofisica de Canarias, the Michigan State/Notre Dame/JINA Participation Group, Johns Hopkins University, Lawrence Berkeley National Laboratory, Max Planck Institute for Astrophysics, Max Planck Institute for Extraterrestrial Physics, New Mexico State University, New York University, Ohio State University, Pennsylvania State University, University of Portsmouth, Princeton University, the Spanish Participation Group, University of Tokyo, University of Utah, Vanderbilt University, University of Virginia, University of Washington, and Yale University.

```
REFERENCES
Andersen M. I., et al., 2000, A&A, 364, L54
Annis J., et al., 2014, ApJ, 794, 120
Antonelli L. A., et al., 2010, GRB Coordinates Network, 10620
Arcavi I., et al., 2011, ApJ, 742, L18
Backer D. C., Fisher J. R., 1974, ApJ, 189, 137
Ball L., Kesteven M. J., Campbell-Wilson D., Turtle A. J.,
   Hjellming R. M., 1995, MNRAS, 273, 722
Barry R. K., Mukai K., Sokoloski J. L., Danchi W. C., Hachisu
   I., Evans A., Gehrz R., Mikolajewska J., 2008, in Evans A.,
   Bode M. F., O'Brien T. J., Darnley M. J., eds, Astronomical
   Society of the Pacific Conference Series Vol. 401, RS Ophiuchi
   (2006) and the Recurrent Nova Phenomenon. p. 52
Barth A. J., et al., 2003, ApJ, 584, L47
Bastian T. S., 1990, Sol. Phys., 130, 265
Bembrick C., Pearce A., Evans R. O., 2001, IAU Circ., 7781, 3
Berger E., Becker G., 2005, GRB Coordinates Network, 3520
Berger E., et al., 2000, ApJ, 545, 56
Berger E., et al., 2001, ApJ, 556, 556
Berger E., Kulkarni S. R., Chevalier R. A., 2002a, ApJ, 577, L5
Berger E., et al., 2002b, ApJ, 581, 981
Berger E., et al., 2003a, Nature, 426, 154
Berger E., Soderberg A. M., Frail D. A., Kulkarni S. R., 2003b,
   ApJ, 587, L5
Berger E., et al., 2005a, Nature, 438, 988
Berger E., et al., 2005b, ApJ, 634, 501
Beswick R. J., Muxlow T. W. B., Argo M. K., Pedlar A., Marcaide
   J. M., Wills K. A., 2005, ApJ, 623, L21
Bloemen S., et al., 2016, in Ground-based and Airborne Tele-
```

```
Bloom J. S., Berger E., Kulkarni S. R., Djorgovski S. G., Frail
   D. A., 2003, AJ, 125, 999
Bloom J. S., Perley D. A., Chen H. W., 2006, GRB Coordinates
   Network, 5826
Bloom J. S., et al., 2009, ApJ, 691, 723
Bloom J. S., et al., 2012, PASP, 124, 1175
Booth R. S., Jonas J. L., 2012, African Skies, 16, 101
Bower G. C., Saul D., Bloom J. S., Bolatto A., Filippenko A. V.,
   Foley R. J., Perley D., 2007, ApJ, 666, 346
Brocksopp C., Jonker P. G., Fender R. P., Groot P. J., van der
   Klis M., Tingay S. J., 2001, MNRAS, 323, 517
Brocksopp C., et al., 2002, MNRAS, 331, 765
Brown T. M., et al., 2013, PASP, 125, 1031
Bufano F., et al., 2014, MNRAS, 439, 1807
Buta R. J., 1982, PASP, 94, 578
Buxton M. M., Bailyn C. D., 2004, ApJ, 615, 880
Buxton M. M., Bailyn C. D., Capelo H. L., Chatterjee R., Dinçer
   T., Kalemci E., Tomsick J. A., 2012, AJ, 143, 130
Cameron P. B., 2005, GRB Coordinates Network, 3513, 1
Cameron P. B., Frail D. A., 2005, GRB Coordinates Network,
   3495
Casares J., Charles P. A., Jones D. H. P., Rutten R. G. M.,
   Callanan P. J., 1991, MNRAS, 250, 712
Castro-Tirado A. J., et al., 1999, Science, 283, 2069
Castro-Tirado A. J., et al., 2001, A&A, 370, 398
Castro S. M., Diercks A., Djorgovski S. G., Kulkarni S. R.,
   Galama T. J., Bloom J. S., Harrison F. A., Frail D. A., 2000,
   GRB Coordinates Network, 605
Castro S., et al., 2001, GRB Coordinates Network, 999
Cenko S. B., Kulkarni S. R., Gal-Yam A., Berger E., 2005, GRB
   Coordinates Network, 3542
Cenko S. B., et al., 2006, ApJ, 652, 490
Cenko S. B., Cucchiara A., Fox D. B., Berger E., Price P. A.,
   2007, GRB Coordinates Network, 6888
Cenko S. B., Perley D. A., Junkkarinen V., Burbidge M., Diego
   U. S., Miller K., 2009, GRB Coordinates Network, 9518
Cenko S. B., et al., 2015, ApJ, 803, L24
Chandra P., Frail D. A., 2006, GRB Coordinates Network, 5843,
Chandra P., Frail D. A., 2007a, GRB Coordinates Network, 6915,
Chandra P., Frail D. A., 2007b, GRB Coordinates Network, 6978,
Chandra P., Frail D. A., 2008a, GRB Coordinates Network, 7843,
Chandra P., Frail D. A., 2008b, GRB Coordinates Network, 8103,
   1
Chandra P., Frail D. A., 2008c, GRB Coordinates Network, 8625,
   1
Chandra P., Frail D. A., 2009a, GRB Coordinates Network, 9260,
Chandra P., Frail D. A., 2009b, GRB Coordinates Network, 9533,
Chandra P., Frail D. A., 2012, ApJ, 746, 156
Chandra P., et al., 2008, ApJ, 683, 924
Chandra P., Frail D. A., Cenko S. B., 2010, GRB Coordinates
   Network, 11131, 1
Chevalier R. A., Fransson C., Nymark T. K., 2006, ApJ, 641, 1029
Chomiuk L., Weston J., Sokoloski J., Nelson T., Rupen M., Mukai
   K., Roy N., Mioduszewski A., 2012, The Astronomer's Tele-
   gram, 4288
Chornock R., Perley D. A., Cenko S. B., Bloom J. S., Cobb B.,
   Prochaska J. X., 2009a, GRB Coordinates Network, 8994
Chornock R., Perley D. A., Cenko S. B., Bloom J. S., 2009b, GRB
   Coordinates Network, 9028
Chornock R., Perley D. A., Cenko S. B., Bloom J. S., 2009c, GRB
   Coordinates Network, 9243
```

scopes VI. p. 990664, doi:10.1117/12.2232522

```
Chornock R., Berger E., Fox D., Levan A. J., Tanvir N. R.,
   Wiersema K., 2010, GRB Coordinates Network, 11164
Clark J. S., et al., 2000, A&A, 356, 50
Clocchiatti A., et al., 2001, ApJ, 553, 886
Clocchiatti A., Suntzeff N. B., Covarrubias R., Candia P., 2011,
   AJ, 141, 163
Cobb B. E., Bailyn C. D., 2005, GRB Coordinates Network, 3104,
Coppejans D. L., Körding E. G., Miller-Jones J. C. A., Rupen
   M. P., Knigge C., Sivakoff G. R., Groot P. J., 2015, MNRAS,
   451, 3801
Corbel S., et al., 2013, MNRAS, 431, L107
Covino S., et al., 2003, A&A, 404, L5
Cucchiara A., Fox D. B., Tanvir N., Berger E., 2009, GRB Coor-
   dinates Network, 9873
Dawson K. S., et al., 2013, AJ, 145, 10
Della Valle M., et al., 2006, ApJ, 642, L103
Dewdney P. E., Hall P. J., Schilizzi R. T., Lazio T. J. L. W., 2009,
   IEEE Proceedings, 97, 1482
Dhillon V. S., Marsh T. R., Littlefair S. P., 2006, MNRAS, 372,
Dhillon V. S., et al., 2011, MNRAS, 414, 3627
Djorgovski S. G., Kulkarni S. R., Bloom J. S., Goodrich R., Frail
   D. A., Piro L., Palazzi E., 1998, ApJ, 508, L17
Djorgovski S. G., et al., 1999, GRB Coordinates Network, 256
Djorgovski S. G., Mahabal A. A., Donalek C., Graham M. J.,
   Drake A. J., Moghaddam B., Turmon M., 2012, preprint,
   (arXiv:1209.1681)
Drout M. R., et al., 2011, ApJ, 741, 97
Drout M. R., et al., 2014, ApJ, 794, 23
Durouchoux P., et al., 1996, IAU Circ., 6383
Eisenstein D. J., et al., 2011, AJ, 142, 72
Eyres S. P. S., et al., 2009, MNRAS, 395, 1533
Farrell S. A., Murphy T., Lo K. K., 2015, ApJ, 813, 28
Fatkhullin T. A., Sokolov V. V., Guziy S., de Ugarte Postigo A.,
   Perez-Ramirez D., Gorosabel J., Jelinek M., Castro-Tirado
   A. J., 2007, GRB Coordinates Network, 6984
Fender R., De Bruyn G., Pooley G., Stappers B., 2004, The As-
   tronomer's Telegram, 361
Fender R., Garrington S., Muxlow T., 2005, The Astronomer's
   Telegram, 558
Fender R., Stewart A., Macquart J.-P., Donnarumma I., Mur-
   phy T., Deller A., Paragi Z., Chatterjee S., 2015, preprint,
   (arXiv:1507.00729)
Ferland G. J., 1977, ApJ, 215, 873
Ferrero P., et al., 2006, A&A, 457, 857
Fox D. B., Kulkarni S. R., 2004, The Astronomer's Telegram, 354
Frail D. A., Berger E., 2002, GRB Coordinates Network, 1490, 1
Frail D. A., Berger E., 2003, GRB Coordinates Network, 1827, 1
Frail D. A., et al., 2000a, ApJ, 534, 559
Frail D. A., Waxman E., Kulkarni S. R., 2000b, ApJ, 537, 191
Frail D. A., et al., 2000c, ApJ, 538, L129
Frail D. A., Kulkarni S. R., Berger E., Wieringa M. H., 2003a,
   AJ, 125, 2299
Frail D. A., et al., 2003b, ApJ, 590, 992
Frail D. A., Cameron P. B., Soderberg A. M., 2005, GRB Coor-
   dinates Network, 4244, 1
Frail D. A., Chandra P., Singh T., 2009, GRB Coordinates Net-
   work, 10088, 1
Frail D. A., Kulkarni S. R., Ofek E. O., Bower G. C., Nakar E.,
   2012, ApJ, 747, 70
Frei Z., Gunn J. E., 1994, AJ, 108, 1476
Fynbo J. U., et al., 2001, A&A, 373, 796
Gaensler B. M., Stappers B. W., Getts T. J., 1999, ApJ, 522,
Gal-Yam A., Ofek E. O., Shemmer O., 2002, MNRAS, 332, L73
```

Gal-Yam A., et al., 2006, ApJ, 639, 331

```
Gal R. R., Bloom J. S., Steidel C., Adelberger K. L., Djorgovski
   S. G., Kulkarni S. R., 1998, GRB Coordinates Network, 88
Galama T. J., et al., 2000, ApJ, 541, L45
Galama T. J., Frail D. A., Sari R., Berger E., Taylor G. B., Kulka-
   rni S. R., 2003, ApJ, 585, 899
Garnavich P. M., et al., 2003, ApJ, 582, 924
Giles A. B., Hill K. M., Greenhill J. G., 1999, MNRAS, 304, 47
Giles A. B., Greenhill J. G., Hill K. M., Sanders E., 2005, MN-
   RAS, 361, 1180
Goranskij V. P., Zharova A. V., 2014, The Astronomer's Tele-
   gram, 6504
Gregory P. C., Xu H.-J., Backhouse C. J., Reid A., 1989, ApJ,
   339, 1054
Greiner J., Peimbert M., Esteban C., Kaufer A., Jaunsen A.,
   Smoke J., Klose S., Reimer O., 2003, GRB Coordinates Net-
   work, 2020
Grupe D., et al., 2006, ApJ, 645, 464
Güdel M., 2002, ARA&A, 40, 217
Guidorzi C., et al., 2011, MNRAS, 417, 2124
Guillochon J., Parrent J., Kelley L. Z., Margutti R., 2017, ApJ,
Halpern J. P., 2005, The Astronomer's Telegram, 549
Halpern J. P., Mirabal N., Armstrong E., 2006, GRB Coordinates
   Network, 5840, 1
Hamuy M., et al., 2009, ApJ, 703, 1612
Han X., Hjellming R. M., 1992, ApJ, 400, 304
Hannikainen D., et al., 2001, in Gimenez A., Reglero V., Win-
   kler C., eds, ESA Special Publication Vol. 459, Explor-
   ing the Gamma-Ray Universe. pp 291-294 (arXiv:astro-
   ph/0102070)
Harrison F. A., et al., 1999, ApJ, 523, L121
Harrison F. A., et al., 2001, ApJ, 559, 123
Harrison F., Cenko B., Frail D. A., Chandra P., Kulkarni S., 2009,
   GRB Coordinates Network, 9043, 1
Haynes R. F., Jauncey D. L., Murdin P. G., Goss W. M., Long-
   more A. J., Simons L. W. J., Milne D. K., Skellern D. J., 1978,
   MNRAS, 185, 661
Heinz S., et al., 2015, ApJ, 806, 265
Hjellming R. M., 1996, in Taylor A. R., Paredes J. M., eds, As-
   tronomical Society of the Pacific Conference Series Vol. 93,
   Radio Emission from the Stars and the Sun. p. 174
Hjellming R. M., Wade C. M., Vandenberg N. R., Newell R. T.,
   1979, AJ, 84, 1619
Hjellming R. M., Calovini T. A., Han X. H., Cordova F. A., 1988,
    ApJ, 335, L75
Hjellming R. M., et al., 2000, ApJ, 544, 977
Hjorth J., et al., 2003, ApJ, 597, 699
Hobbs G., et al., 2004, MNRAS, 352, 1439
Hodge J. A., Becker R. H., White R. L., Richards G. T., Zeimann
   G. R., 2011, AJ, 142, 3
Høg E., et al., 2000, A&A, 355, L27
Horesh A., et al., 2013, MNRAS, 436, 1258
Hunter D. J., et al., 2009, A&A, 508, 371
Im M., Lee I., Urata Y., 2007, GRB Coordinates Network, 6970,
Im M., Jeon Y., Park W., Lee I., Jeon Y.-B., Urata Y., 2009,
   GRB Coordinates Network, 9275, 1
Ivezic Z., et al., 2008, preprint, (arXiv:0805.2366)
Jain R. K., Bailyn C. D., Orosz J. A., Remillard R. A., McClin-
   tock J. E., 1999, ApJ, 517, L131
Jensen B. L., et al., 1999, GRB Coordinates Network, 498
Johnston S., Romani R. W., Marshall F. E., Zhang W., 2004,
```

MNRAS, 355, 31

Johnston S., et al., 2008, Experimental Astronomy, 22, 151 Jonker P. G., Nelemans G., Bassa C. G., 2007, MNRAS, 374, 999

Kalemci E., Begelman M. C., Maccarone T. J., Dincer T., Russell

T. D., Bailyn C., Tomsick J. A., 2016, MNRAS, 463, 615

```
Kaluzienski L., Holt S., Canizares C., McClintock J., Grindlay J.,
   Liller M., Stryker L., 1979, IAU Circ., 3362
Kann D. A., Hoegner C., Filgas R., 2007, GRB Coordinates Net-
   work, 6918, 1
Kantor J., 2014, in Wozniak P. R., Graham M. J., Mahabal A. A.,
   Seaman R., eds, The Third Hot-wiring the Transient Universe
   Workshop. pp 19–26
Kasliwal M. M., 2011, Bulletin of the Astronomical Society of
   India, 39, 375
Kato M., Hachisu I., 2005, ApJ, 633, L117
Kato T., Uemura M., Ishioka R., Nogami D., Kunjaya C., Baba
   H., Yamaoka H., 2004, PASJ, 56, S1
Kellermann K. I., 1966, ApJ, 146, 621
Kelson D., Berger E., 2005, GRB Coordinates Network, 3101
Kemp J. C., Karitskaya E. A., Kumsiashvili M. I., Lyutyi V. M.,
   Khruzina T. S., Cherepashchuk A. M., 1987, Soviet Ast., 31,
Körding E., Rupen M., Knigge C., Fender R., Dhawan V., Tem-
   pleton M., Muxlow T., 2008, Science, 320, 1318
Körding E. G., Knigge C., Tzioumis T., Fender R., 2011, MNRAS,
Krauss M. I., et al., 2011, ApJ, 739, L6
Kulkarni S. R., et al., 1998, Nature, 395, 663
Kulkarni S. R., et al., 1999, ApJ, 522, L97
Lamb D. Q., Castander F. J., Reichart D. E., 1999, A&AS, 138,
Law N. M., et al., 2009, PASP, 121, 1395
Ledoux C., et al., 2005, GRB Coordinates Network, 3860
Lee M. G., Kim E., Kim S. C., Kim S. L., Park W.-K., Pyo T. S.,
   1995, Journal of Korean Astronomical Society, 28, 31
Lennarz D., Altmann D., Wiebusch C., 2012, A&A, 538, A120
Leonard D. C., et al., 2002, PASP, 114, 35
Levan A., et al., 2006, ApJ, 647, 471
Levinson A., Ofek E. O., Waxman E., Gal-Yam A., 2002, ApJ,
   576, 923
Lipkin Y. M., et al., 2004, ApJ, 606, 381
Liu Q. Z., van Paradijs J., van den Heuvel E. P. J., 2006, A&A,
   455, 1165
Liu Q. Z., van Paradijs J., van den Heuvel E. P. J., 2007, A&A,
   469, 807
Lo K. K., Farrell S., Murphy T., Gaensler B. M., 2014, ApJ, 786,
Lorimer D. R., Yates J. A., Lyne A. G., Gould D. M., 1995,
   MNRAS, 273, 411
Mahabal A. A., et al., 2011, Bulletin of the Astronomical Society
   of India, 39, 387
Malesani D., et al., 2007, A&A, 473, 77
Manchester R. N., Hobbs G. B., Teoh A., Hobbs M., 2005, AJ,
   129, 1993
Marshall F. E., et al., 2011, ApJ, 727, 132
Marti J., Paredes J. M., Ribo M., 1998, A&A, 338, L71
Masetti N., et al., 2003, A&A, 404, 465
Mazzali P. A., et al., 2008, Science, 321, 1185
Melandri A., et al., 2010, ApJ, 723, 1331
Metzger B. D., Williams P. K. G., Berger E., 2015, ApJ, 806, 224
Migliari S., et al., 2010, ApJ, 710, 117
Mignani R. P., 2011, Advances in Space Research, 47, 1281
Miller-Jones J. C. A., Sivakoff G. R., 2013, The Astronomer's
   Telegram, 5148
Miller-Jones J. C. A., Jonker P. G., Dhawan V., Brisken W., Ru-
   pen M. P., Nelemans G., Gallo E., 2009, ApJ, 706, L230
Mirabal N., Halpern J. P., 2006, GRB Coordinates Network, 4792
Mirabel I. F., Marti J., Duc P. A., Rodriguez L. F., Duerbeck H.,
   Benetti S., 1996, IAU Circ., 6427
```

Misra K., Kamble A. P., Sahu D. K., Srividya S., Bama P., Anupama G. C., Vanniarajan M. S., 2005, GRB Coordinates Net-

```
Misra K., Pooley D., Chandra P., Bhattacharya D., Ray A. K.,
   Sagar R., Lewin W. H. G., 2007a, MNRAS, 381, 280
Misra K., Pooley D., Chandra P., Bhattacharya D., Ray A. K.,
   Sagar R., Lewin W. H. G., 2007b, MNRAS, 381, 280
Moin A., et al., 2013, ApJ, 779, 105
Moody J. W., Laney D., Pearson R., Pace C., 2010, GRB Coor-
   dinates Network, 10665, 1
Mooley K. P., et al., 2016, ApJ, 818, 105
Munari U., Walter F. M., Henden A., Dallaporta S., Finzell T.,
   Chomiuk L., 2015, Information Bulletin on Variable Stars,
Nagashima M., et al., 2013, in Di Stefano R., Orio
   M., Moe M., eds, IAU Symposium Vol. 281, Binary
   Paths to Type Ia Supernovae Explosions. pp 121-123,
   \mathrm{doi:} 10.1017/\mathrm{S}1743921312014810
Nardini M., et al., 2014, A&A, 562, A29
Nelson T., et al., 2014, ApJ, 785, 78
O'Meara J., Chen H.-W., Prochaska J. X., 2010, GRB Coordi-
   nates Network, 11089
Ofek E. O., Breslauer B., Gal-Yam A., Frail D., Kasliwal M. M.,
    Kulkarni S. R., Waxman E., 2010, ApJ, 711, 517
Ofek E. O., Frail D. A., Breslauer B., Kulkarni S. R., Chandra
   P., Gal-Yam A., Kasliwal M. M., Gehrels N., 2011, ApJ, 740,
   65
Olausen S. A., Kaspi V. M., 2014, ApJS, 212, 6
Oosterloo T., Verheijen M., van Cappellen W., 2010, in
   ISKAF2010 Science Meeting. p. 43 (arXiv:1007.5141)
Owen F. N., Balonek T. J., Dickey J., Terzian Y., Gottesman
   S. T., 1976, ApJ, 203, L15
Özdönmez A., Güver T., Cabrera-Lavers A., Ak T., 2016, MN-
   RAS, 461, 1177
Page K. L., et al., 2009, MNRAS, 400, 134
Palazzi E., et al., 1998, A&A, 336, L95
Panagia N., Sramek R. A., Weiler K. W., 1986, ApJ, 300, L55
Pandey S. B., et al., 2010, ApJ, 714, 799
Pâris I., et al., 2012, A&A, 548, A66
Park S. Q., et al., 2004, ApJ, 610, 378
Perley D. A., 2009a, GRB Coordinates Network, 9042, 1
Perley D. A., 2009b, GRB Coordinates Network, 10058, 1
Perley D. A., Bloom J. S., 2008, GRB Coordinates Network, 8631,
Perley D. A., et al., 2008, ApJ, 688, 470
Perley R. A., Chandler C. J., Butler B. J., Wrobel J. M., 2011,
   ApJ, 739, L1
Perryman M. A. C., et al., 1997, A&A, 323, L49
Pietka M., Fender R. P., Keane E. F., 2015, MNRAS, 446, 3687
Pietka M., Staley T. D., Pretorius M. L., Fender R. P., 2017,
   MNRAS, 471, 3788
Pignata G., et al., 2011, ApJ, 728, 14
Pooley D., et al., 2002, ApJ, 572, 932
Pozzo M., et al., 2006, MNRAS, 368, 1169
Price P. A., et al., 2002a, ApJ, 571, L121
Price P. A., et al., 2002b, ApJ, 572, L51
Price P. A., et al., 2002c, ApJ, 573, 85
Prieto J. L., Watson L. C., Stanek K. Z., 2009, The Astronomer's
   Telegram, 2065
Qiu Y., Li W., Qiao Q., Hu J., 1999, AJ, 117, 736
Quimby R., Fox D., Hoeflich P., Roman B., Wheeler J. C., 2005,
   GRB Coordinates Network, 4221
Rahmer G., Smith R., Velur V., Hale D., Law N., Bui
   K., Petrie H., Dekany R., 2008, in Ground-based and
   Airborne Instrumentation for Astronomy II. p. 70144Y,
   doi:10.1117/12.788086
Raiteri C. M., et al., 2011, A&A, 534, A87
```

Ramsay G., Schreiber M., Gansicke B., Wheatley P., 2017,

preprint, (arXiv:1704.00496)

Rau A., et al., 2009, PASP, 121, 1334

work, 4259, 1

Rebbapragada U., Lo K., Wagstaff K. L., Reed C., Murphy T., Thompson D. R., 2012, in Griffin E., Hanisch R., Seaman R., eds, IAU Symposium Vol. 285, New Horizons in Time Domain Astronomy. pp 397–399, doi:10.1017/S1743921312001196

Reig P., Fabregat J., 2015, A&A, 574, A33

Rhoads J. E., Fruchter A. S., 2001, ApJ, 546, 117

Richards G. T., et al., 2009, ApJS, 180, 67

Richards J. W., et al., 2011, ApJ, 733, 10

Richmond M. W., et al., 1996a, AJ, 111, 327

Richmond M. W., Treffers R. R., Filippenko A. V., Paik Y., 1996b, AJ, 112, 732

Romero-Cañizales C., et al., 2014, MNRAS, 440, 1067

Roming P. W. A., et al., 2009, ApJ, 704, L118

Rowlinson A., et al., 2016, MNRAS,

Roy R., et al., 2013, MNRAS, 434, 2032

Rumyantsev V., Pozanenko A., 2009, GRB Coordinates Network, 9539, 1

Rumyantsev V., Shakhovkoy D., Pozanenko A., 2010, GRB Coordinates Network, 11255, 1

Rupen M. P., Dhawan V., Mioduszewski A. J., 2002, IAU Circ.,

Ryder S. D., Sadler E. M., Subrahmanyan R., Weiler K. W., Panagia N., Stockdale C., 2004, MNRAS, 349, 1093

Sagar R., et al., 2001, Bulletin of the Astronomical Society of India, 29, 91

Saglia R. P., et al., 2012, ApJ, 746, 128

Salas P., Bauer F. E., Stockdale C., Prieto J. L., 2013, MNRAS, 428, 1207

Sánchez-Fernández C., et al., 1999, A&A, 348, L9

Schlafly E. F., Finkbeiner D. P., 2011, ApJ, 737, 103

Schmeer P., Hornoch K., Lehky M., 2004, IAU Circ., 8379, 2

Schneider D. P., et al., 2007, AJ, 134, 102

Schneider D. P., et al., 2010, AJ, 139, 2360

Shaposhnikov N., Swank J., Shrader C. R., Rupen M., Beckmann V., Markwardt C. B., Smith D. A., 2007, ApJ, 655, 434

Shrader C. R., Wagner R. M., Hjellming R. M., Han X. H., Starrfield S. G., 1994, ApJ, 434, 698

Sobczak G. J., McClintock J. E., Remillard R. A., Levine A. M., Morgan E. H., Bailyn C. D., Orosz J. A., 1999, ApJ, 517, L121

Soderberg A. M., 2005, GRB Coordinates Network, 3187, 1

Soderberg A. M., Kulkarni S. R., Berger E., Chevalier R. A., Frail D. A., Fox D. B., Walker R. C., 2005, ApJ, 621, 908

Soderberg A. M., et al., 2006a, Nature, 442, 1014

Soderberg A. M., et al., 2006b, ApJ, 650, 261

Soderberg A. M., Chevalier R. A., Kulkarni S. R., Frail D. A., 2006c, ApJ, 651, 1005

Soderberg A., Chandra P., Frail D., 2008, GRB Coordinates Network, 7506

Soderberg A. M., et al., 2010a, Nature, 463, 513

Soderberg A. M., Brunthaler A., Nakar E., Chevalier R. A., Bietenholz M. F., 2010b, ApJ, 725, 922

Sokoloski J. L., Crotts A. P. S., Lawrence S., Uthas H., 2013, ApJ,

Sokolov V. V., Kopylov A. I., Zharikov S. V., Feroci M., Nicastro L., Palazzi E., 1998, A&A, 334, 117

Steele I. A., et al., 2004, in Oschmann Jr. J. M., ed., Society of Photo-Optical Instrumentation Engineers (SPIE) Conference Series Vol. 5489, Ground-based Telescopes. pp 679–692, doi:10.1117/12.551456

Stewart A. J., et al., 2016, MNRAS, 456, 2321

Stockdale C. J., et al., 2002, IAU Circ., 8018, 1

Stockdale C. J., Sramek R. A., Weiler K. W., van Dyk S. D., Panagia N., Pooley D., Lewin W., Marcaide J. M., 2004a, IAU Circ., 8379, 1

Stockdale C. J., Weiler K. W., van Dyk S. D., Sramek R. A., Panagia N., Marcaide J. M., 2004b, IAU Circ., 8415, 1

Taylor A. R., Jarvis M., 2017, IOP Conference Series: Materials Science and Engineering, 198, 012014

Taylor G. B., Frail D. A., Kulkarni S. R., Shepherd D. S., Feroci M., Frontera F., 1998, ApJ, 502, L115

Thyagarajan N., Helfand D. J., White R. L., Becker R. H., 2011, ApJ, 742, 49

Tingay S. J., et al., 2013, Publ. Astron. Soc. Australia, 30, e007 Tonry J. L., et al., 2012, ApJ, 745, 42

Trushkin S. A., Nizhelskij N. A., Tsybulev P. G., 2014, The Astronomer's Telegram, 6492

Tsvetkov D. Y., 1987, Soviet Astronomy Letters, 13, 376

Tsvetkov D. Y., Goranskij V., Pavlyuk N., 2008, Peremennye Zvezdy, 28

Turatto M., Cappellaro E., Danziger I. J., Benetti S., Gouiffes C., della Valle M., 1993, MNRAS, 262, 128

Uemura M., Kato T., Pavlenko E., Shugarov S., Mitskevich M., Fried R. E., Sano Y., 2004, PASJ, 56, S147

Updike A. C., et al., 2008, ApJ, 685, 361

Vanden Berk D. E., et al., 2001, AJ, 122, 549

Veillet C., 2000, GRB Coordinates Network, 588

Villata M., et al., 2009, A&A, 501, 455

Vreeswijk P. M., et al., 2001, ApJ, 546, 672

Vreeswijk P. M., et al., 2006, A&A, 447, 145

Vreeswijk P. M., Smette A., Malesani D., Fynbo J. P. U., Milvang-Jensen B., Jakobsson P., Jaunsen A. O., Ledoux C., 2008, GRB Coordinates Network, 7444

Watson D., et al., 2006, ApJ, 652, 1011

Weiler K. W., Sramek R. A., Panagia N., van der Hulst J. M., Salvati M., 1986, ApJ, 301, 790

Weiler K. W., Williams C. L., Panagia N., Stockdale C. J., Kelley M. T., Sramek R. A., Van Dyk S. D., Marcaide J. M., 2007, ApJ, 671, 1959

Weiler K. W., Panagia N., Stockdale C., Rupen M., Sramek R. A., Williams C. L., 2011, ApJ, 740, 79

Wellons S., Soderberg A. M., Chevalier R. A., 2012, ApJ, 752, 17 Wendker H. J., 1995, A&AS, 109, 177

Whelan J. A. J., et al., 1977, MNRAS, 180, 657

White R. L., Becker R. H., Helfand D. J., Gregg M. D., 1997, ApJ, 475, 479

Williams C. L., Panagia N., Van Dyk S. D., Lacey C. K., Weiler K. W., Sramek R. A., 2002, ApJ, 581, 396

Williams P. K. G., Bower G. C., Croft S., Keating G. K., Law C. J., Wright M. C. H., 2013, ApJ, 762, 85

Woodsworth A. W., Higgs L. A., Gregory P. C., 1980, A&A, 84,

Wright A., Otrupcek R., 1990, in PKS Catalog (1990). p. 0

Xu D., et al., 2009, GRB Coordinates Network, 10053

Yokoo T., Arimoto J., Matsumoto K., Takahashi A., Sadakane K., 1994, PASJ, 46, L191

York D. G., et al., 2000, AJ, 120, 1579

Young D. R., et al., 2010, A&A, 512, A70

della Valle M., Jarvis B. J., West R. M., 1991, A&A, 247, L33

della Valle M., Mirabel I. F., Rodriguez L. F., 1994, A&A, 290, 803

van Dyk S. D., Sramek R. A., Weiler K. W., Panagia N., 1993, ApJ, 409, 162

van Dyk S. D., Sramek R. A., Montes M. J., Weiler K. W., Panagia N., 1996, IAU Circ., 6528, 1

van Haarlem M. P., et al., 2013, A&A, 556, A2

van Leeuwen F., 2007, A&A, 474, 653

van der Horst A. J., Kamble A. P., Wijers R. A. M. J., Kouveliotou C., 2009, GRB Coordinates Network, 9883, 1

van der Horst A. J., Wiersema K., Kamble A. P., Wijers R. A. M. J., Rol E., Kouveliotou C., 2010, GRB Coordinates Network, 11221, 1

van der Horst A. J., et al., 2011, ApJ, 726, 99

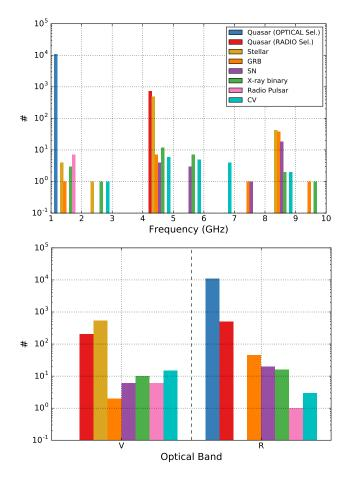


Figure A1. Upper panel: The distribution of radio frequencies used for the F_r measurements collected for each class of object in the sample. Each bin is a width of 1 GHz. Lower panel: The distribution of optical bands used for the F_0 measurements collected for each class of object in the sample. The legend in the upper plot also applies to the lower.

APPENDIX A: SAMPLE FREQUENCY/BAND DISTRIBUTION AND REFERENCE TABLES

Fig. A1 shows the distribution of the radio frequencies and optical bands used for the sample, for each class of object. The redshift distribution of the quasar sample is shown in Fig. A2, followed by the distribution of the parallax distance measurements of the stellar sample in Fig. A3. Fig. A4 shows the redshift distribution of the GRB sample. Tables A1, A2, A3, A4 and A5 provide the references for the F_0 and F_r measurements for our sample of radio pulsars, CVs, XRBs, SNe, and GRBs, respectively.

This paper has been typeset from a TEX/IATEX file prepared by the author.

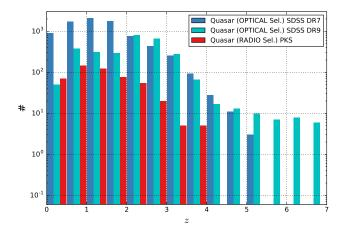


Figure A2. The distribution of redshifts for the quasar sample, complied from the Seventh Data Release quasar catalogue (DR7QC; Schneider et al. 2010), the Ninth Data Release quasar catalogue (DR9QC; Pâris et al. 2012) and the Parkes Survey (Wright & Otrupcek 1990). Note that not all redshifts were available for the Parkes survey.

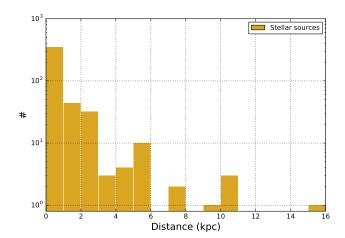


Figure A3. The distribution of the parallax distance measurements of the stellar sample compiled using the data presented in (Güdel 2002).

Table A1. The radio pulsars that are included in the sample. The radio measurements and distances were gathered with the use of the ATNF Pulsar Catalogue (Manchester et al. 2005).

Object Name	$F_{\rm o}$ ref.	$F_{\rm r}$ ref.	d (kpc)
Crab (B0531+21)	Mignani (2011)	Lorimer et al. (1995)	2.00
Vela (B0833-45)	Mignani (2011)	Backer & Fisher (1974)	0.28
B0540-69	Mignani (2011)	Johnston et al. (2004)	49.70
B1509-58	Mignani (2011)	Hobbs et al. (2004)	4.40
B0656 + 14	Mignani (2011)	Lorimer et al. (1995)	0.29
B1133+16	Mignani (2011)	Lorimer et al. (1995)	0.35
B0950+08	Mignani (2011)	Lorimer et al. (1995)	02.6

Table A2. The CVs that are included in the sample. The first section contains CVs obtained from the Stellar sample (see Section 2.3). The second section contains CVs obtained from the data contained in Pietka et al. (2015) which are all flaring nova events. The third section are two sources gathered manually and the final section contains CVs from Coppejans et al. (2015). The distance references are as follows: [1] van Leeuwen (2007); [2] Özdönmez et al. (2016); [3] Barry et al. (2008); [4] Munari et al. (2015); [5] Sokoloski et al. (2013); [6] Ferland (1977); [7] Krauss et al. (2011); [8] Kato & Hachisu (2005); [9] Ramsay et al. (2017); [10] Coppejans et al. (2015). Below the table are notes on individual sources regarding the circumstance of the F_0 and F_r measurements used. If no note is present for a source it can be assumed to be in quiescence.

Object Name	CV Subclass	$F_{\rm o}$ ref.	$F_{\rm r}$ ref.	d (pc)
T CrB	Nova	Güdel (2002)	Güdel (2002)	1,063.8 [1]
V* RT Ser	Nova	Güdel (2002)	Güdel (2002)	$\geq 1,200 [2]$
RS Oph^a	Nova	Güdel (2002)	Güdel (2002)	1,400 [3]
V 4074 Sgr	Nova	Güdel (2002)	Güdel (2002)	-
HM Sge	Nova	Güdel (2002)	Güdel (2002)	$\geq 1,500 [2]$
PU Vul	Nova	Güdel (2002)	Güdel (2002)	-
AG Peg	Nova	Güdel (2002)	Güdel (2002)	-
Nova Sco 2012	Nova	Munari et al. (2015)	Chomiuk et al. (2012)	3,700-4,300 [4]
T Pyx	Nova	Nelson et al. (2014)	Nelson et al. (2014)	4800 [5]
V1500 Cyg	Nova	AAVSO	Hjellming et al. (1979)	1950 [6]
V1723 Aql	Nova	Nagashima et al. (2013)	Krauss et al. (2011)	5000 [7]
V1974 Cyg	Nova	AAVSO	Hjellming (1996)	1830 [8]
SS Cyg	Dwarf Nova	Körding et al. (2008)	Körding et al. (2008)	117.1 [9]
V3885 Sgr	Dwarf Nova	AAVSO	Körding et al. (2011)	136.0 [9]
RW Sex	Novalike	Coppejans et al. (2015)/AAVSO	Coppejans et al. (2015)	150.0 [10]
V603 Aql	Novalike	Coppejans et al. (2015)/AAVSO	Coppejans et al. (2015)	328.3 [9]
$\mathrm{TT}\;\mathrm{Ari}^{ar{b}}$	Novalike	Coppejans et al. (2015)/AAVSO	Coppejans et al. (2015)	228.8 [9]

^a Data for RS Oph was also obtained from different sources for the dynamic sample (Table 2).

Notes on the circumstance of the F_0 and F_T measurements obtained for specific sources (refer to main text in Section 2.5 for those without a note):

RS Oph (Dynamic): RS Oph is coverage of a flare that begun on 2006 February 12 and was first detected in the radio 4 d after the optical peak (day 0). **Nova Sco 2012:** The F_0 and F_r measurements were recorded 35 d after the discovery of the nova as an optical transient on 2012 May 22. This was the first radio detection, and it was made after the optical maximum.

T Pyx: The F_0 and F_r measurements used are 66 d after the optical transient discovery on 2011 April 14. This was the first radio detection at 5 GHz. The radio peak occurred ~250 d post discovery.

V1500 Cyg: The F_0 and F_r measurements used are 27 d after the optical transient discovery on 1975 August 28. This was the first radio detection at 8 GHz. The radio peak occurred ~106 d post discovery.

V1723 Cyg: The F_0 and F_r measurements used are 3 d after the optical transient discovery on 2010 September 11. This was the first radio detection at 5 GHz. The radio peak occurred \sim 57 d post discovery.

V1974 Cyg: The F_0 and F_r measurements used are 21 d after the optical transient discovery on 1992 February 19. This was the first radio detection at 8.4 GHz. The radio peak occurred ~250 d post discovery.

SS Cyg: The F_0 and F_r measurements used are 1.3 d after the optical flare was detected on 2007 April 13. This was at the radio peak of the observations which then declined over the next 20 d back to below the detection threshold.

V3885 Sgr: Targeted radio observation with a single detection, matched with optical 38 d later as assumed to be in a quiescent state. TT Ari: Two measurements are included here as one of the targeted radio observations performed by the authors happened to detect a radio flare showing an increase in peak flux density of 200 μ Jy from the previous detection at 40 μ Jy.

 $^{^{}b}$ Two measurements were included in the sample of TT Ari - at radio outburst and quiescence.

Table A3. The XRB sources that are included in the sample. The sample was gathered with the use of two catalogues: the Catalogue of high-mass X-ray binaries in the Galaxy (4^{th} edition; Liu et al. 2006), that accounts for the first section of the table, and the Catalogue of low-mass X-ray binaries in the Galaxy, LMC, and SMC (4^{th} edition; Liu et al. 2007) which accounts for the second section of the table. If the distance does not have an associated reference then it was collected from the respective catalouge. In other cases the distance references are as follows: [1] Heinz et al. (2015); [2] Sánchez-Fernández et al. (1999); [3] Sobczak et al. (1999); [4] Miller-Jones et al. (2009). Below the table are notes on the circumstance of the collected F_0 and F_r measurements for each individual source.

Object Name	Subclass	$F_{ m o}$ ref.	$F_{\rm r}$ ref.	d (kpc)
LS I +61 303	HMXB	Reig & Fabregat (2015)	Gregory et al. (1989)	2.4
XTE J0421+560	HMXB	Clark et al. (2000)	Clark et al. (2000)	1 - 5
SAX J1819.3-2525	HMXB	Hjellming et al. (2000)	Hjellming et al. (2000)	7 - 12
RX J1826.2-1450	HMXB	Marti, Paredes & Ribo (1998)	Marti et al. (1998)	2.5
SS433	HMXB	Goranskij & Zharova (2014)	Trushkin, Nizhelskij & Tsybulev (2014)	5.5
4U 1956+35	HMXB	Kemp et al. (1987)	Woodsworth, Higgs & Gregory (1980)	2.2
IGR J00291+5934	LMXB	Fox & Kulkarni (2004)	Fender et al. (2004)	2.6 - 3.6
GRO J0422+32	LMXB	Shrader et al. (1994)	Shrader et al. (1994)	2.4
$4U\ 0614+091$	LMXB	Migliari et al. (2010)	Migliari et al. (2010)	< 4
1A 0620-00	LMXB	Whelan et al. (1977)	Owen et al. (1976)	1.2
XTE J0929-314	LMXB	Giles et al. (2005)	Rupen, Dhawan & Mioduszewski (2002)	5 - 15
GS 1124-684	LMXB	Ball et al. (1995)	della Valle et al. (1991)	5.9
GS 1354-64	LMXB	Brocksopp et al. (2001)	Brocksopp et al. (2001)	≥ 27
4U 1456-32	LMXB	Kaluzienski et al. (1979)	Hjellming et al. (1988)	1.2
3A 1516-569	$LMXB^a$	Haynes et al. (1978)	Haynes et al. (1978)	8.4 - 10.2 [1]
4U 1543-47	LMXB	Buxton & Bailyn (2004)	Park et al. (2004)	7.5
XTE J1550-564	LMXB	Jain et al. (1999)	Hannikainen et al. (2001)	2.5 - 6 [2,3]
GRO J1655-40	LMXB	Kalemci et al. (2016) (SMARTS ^{b})	Shaposhnikov et al. (2007); Kalemci et al. (2016)	3.2
GX 339-4	LMXB	Buxton et al. (2012)	Corbel et al. (2013)	8.0 [2]
GRO J1719-24	LMXB	della Valle, Mirabel & Rodriguez (1994)	della Valle et al. (1994)	~ 2.4
GRS 1739-278	LMXB	Mirabel et al. (1996)	Durouchoux et al. (1996)	8.5
Swift J1753.5-0127	LMXB	Halpern (2005)	Fender, Garrington & Muxlow (2005)	~ 6
SAX J1808.4-3658	LMXB	Giles, Hill & Greenhill (1999)	Gaensler, Stappers & Getts (1999)	2-5-3.6
XTE J1859+226	LMXB	Uemura et al. (2004)	Brocksopp et al. (2002) (GBI)	7.6
Aql X-1	LMXB	$SMARTS^a$	Miller-Jones & Sivakoff (2013)	5.2
V404 Cygni	LMXB	Casares et al. (1991)	Han & Hjellming (1992)	2.4 [4]

^a The exact nature of the companion of 3A 1516-569 (Cir X-1) is not well known (e.g. Jonker, Nelemans & Bassa (2007)), so while it is in the LMXB catalogue, it is classed as a HMXB in other sources.

Notes on the circumstance of the $F_{\rm 0}$ and $F_{\rm r}$ measurements obtained for each source:

LS I +61~303: Measurements are averages of long-term monitoring (~ 2 months) with no flaring.

XTE J0421+560: 4 d after the detection as an X-ray transient by the Rossi X-ray Timing Explorer (RXTE) on 1998 March 31. Radio peak is used.

SAX J1819.3-2525: Less then 1 d after the detection of an X-ray flare by RXTE on 1999 September 15. Radio peak is used.

RX J1826.2-1450: Targeted radio detection. F_0 measured 26 d prior. Low level variabilty at time of measurements (10 per cent radio, 0.05 mag optical). **SS433:** Radio flare detected on 2014 September 23. F_0 recorded previous day (< 0.5 d).

4U 1956+35: Measurements from two separate long-term monitoring campaings that overlapped in 1977. No flaring seen at time of used measurements. IGR J00291+5934: F_0 and F_1 measurements taken 2 d and 4.5 d, respectively, after X-ray transient detection by INTEGRAL on 2004 December 02.

GRO J0422+32: Approximately 2 weeks after X-ray transient detection by the BATSE experiment on 1992 August 05.

4U 0614+091: Multiwavelength campaign to measure the spectrum. F_0 and F_1 are 2.5 d apart with no major flaring event.

1A 0620-00: Measurements approximately 2 weeks after the detection as an X-ray transient on 1975 August 03.

XTE J0929-314: F_0 and F_r measurements taken 4 d after X-ray transient detection by RXTE on 2002 April 30.

GS 1124-684: F_0 and F_Γ measurements taken 10 d after the discovery as an X-ray transient on 1991 January 08 by the GRANAT satellite. Radio peak is used.

 $\mathbf{GS} \ \mathbf{1354\text{-}64:} \ F_0 \ \mathrm{and} \ F_T \ \mathrm{measurements} \ \mathrm{taken} \ \mathrm{following} \ \mathrm{the} \ \mathrm{detection} \ \mathrm{of} \ \mathrm{a} \ \mathrm{hard\text{-}state} \ \mathrm{outburst} \ \mathrm{in} \ 1997 \ \mathrm{November}, \ \mathrm{mostly} \ \mathrm{in} \ \mathrm{the} \ \mathrm{decay} \ \mathrm{phase}.$

4U 1456-32: F₀ and F_r measurements taken 10 d and 14 d, respectively, after X-ray transient detection by the Ariel 5 all-sky monitor on 1979 May 11.

3A 1516-569: Simultaneous F_0 and $F_{\rm r}$ measurements during a flare on 1977 May 12, very close to radio peak.

4U 1543-47: F₀ and F_r measurements taken 1d after an X-ray outburst was detected by RXTE on 2002 June 16.

XTE J1550-564: Measurements used are at the radio peak, approximately 2 weeks after discovery as an X-ray transient by RXTE on 1998 September 07. GRO J1655-40: Measurements taken at the radio peak which was approximately 1 month after the RXTE detection of an outburst on 2005 February 17. GX 339-4: Measurements taken on 2011 Feb 06 during the decay of an outburst early in the previous year 2010.

 $\textbf{GRO J1719-24:} \ F_{r} \ \text{and} \ F_{0} \ \text{measurements taken 8 d and 10 d, respectively, after X-ray transient detection by BATSE on 1993 September 25.}$

GRS 1739-278: F_0 and F_f measurements taken approximately 1 month after X-ray transient detection on 1996 March 18.

Swift J1753.5-0127: F_0 and F_1 measurements taken 2 d and 3 d, respectively, after new gamma source detection by Swift BAT on 2005 June 30.

SAX J1808.4-3658: F_0 and F_r measurements taken 18 d after an outburst was detected by RXTE on 1998 April 09.

XTE_J1859+226: F₀ and F_r measurements taken 7 d after X-ray transient detection by RXTE on 1999 October 07. This was the radio peak.

Aql X-1: F_0 and F_r measurements taken 15 d after the detection of an outburst in the optical on 2013 June 4. V404 Cygni: F_0 and F_r measurements taken 9 d after X-ray outburst detection on 1989 May 21. This was the radio peak.

Optical and IR monitoring of X-ray binaries using SMARTS (Buxton et al. 2012).

24 Stewart et al.

Table A4. The SN events that are included in this work. The age column signifies the approximate time elapsed since the accepted explosion date of the respective SN. The sample is based upon the list of radio SNe compiled by Romero-Cañizales et al. (2014). The distance references are as follows: [1] Lennarz et al. (2012) and [2] Guillochon et al. (2017).

SN Name	SN Type	$F_{ m o}$ ref.	$F_{ m r}$ ref.	Age (d)	d_L (Mpc)
SN 1980K	IIb	Buta (1982)	Weiler et al. (1986)	37	4.7 [1]
SN 1984L	Ib	Tsvetkov (1987)	Panagia, Sramek & Weiler (1986)	36	18.0 [1]
SN 1988Z	IIn	Turatto et al. (1993)	Williams et al. (2002)	743	70.0 [1]
SN 1990B	Ic	Clocchiatti et al. (2001)	van Dyk et al. (1993)	61	24.0[1]
SN 1993J	II	Richmond et al. (1996b)	Weiler et al. (2007)	11	2.9 [1]
SN 1994I	Ic	Richmond et al. (1996a)	Weiler et al. (2011)	5	6.1 [1]
SN 1996cb	IIb	Qiu et al. (1999)	van Dyk et al. (1996)	9	3.8 [1]
SN 1998bw	Ic	Clocchiatti et al. (2011)	Kulkarni et al. (1998)	16	37.9[2]
SN 1999em	IIP	Leonard et al. (2002)	Pooley et al. (2002)	34	7.7[1]
SN 2001ig	IIb	Bembrick, Pearce & Evans (2001)	Ryder et al. (2004)	12	9.0 [1]
SN 2002ap	Ic	Gal-Yam et al. (2002)	Berger et al. (2002a)	4	3.4[1]
SN 2002hh	II	Pozzo et al. (2006)	Stockdale et al. (2002)	17	4.7[1]
SN 2003L	Ic	$VSNET^a$	Soderberg et al. (2005)	32	95.3[2]
SN 2003bg	IIb	Hamuy et al. (2009)	Soderberg et al. (2006c)	10	20.3[2]
SN 2004dj	IIP	Schmeer, Hornoch & Lehky (2004)	Stockdale et al. (2004a)	23	3.5 [1]
SN 2004dk	Ib	Drout et al. (2011)	Wellons et al. (2012)	8	20.0[1]
SN 2004et	II	Misra et al. (2007b)	Stockdale et al. (2004b)	14	4.7 [1]
SN 2004gq	Ib	Drout et al. (2011)	Wellons et al. (2012)	8	16.0[1]
SN 2007bg	$_{ m Ic}$	Young et al. (2010)	Salas et al. (2013)	19	154.0 [2]
SN 2007gr	Ic	Hunter et al. (2009)	Soderberg et al. (2010b)	5	10.0[1]
SN 2007uy	Ib	Roy et al. (2013)	Roy et al. (2013)	9	26.0[1]
SN 2008D	Ib	Mazzali et al. (2008)	van der Horst et al. (2011)	19	26.0[1]
SN 2008ax	IIb	Roming et al. (2009)	Roming et al. (2009)	8	5.1 [1]
SN 2009bb	Ic	Pignata et al. (2011)	Soderberg et al. (2010a)	20	46.4[2]
SN 2011hs	IIb	Bufano et al. (2014)	Bufano et al. (2014)	12	25.3 [2]
SN~2011dh	IIb	Arcavi et al. (2011)	Horesh et al. (2013)	3	7.3 [2]

 $^{^{}a}$ Variable Star Network (VSNET; Kato et al. 2004)

Table A5. GRB data included in this work which is based upon the list of radio GRB-afterglows compiled by Chandra & Frail (2012). All are long GRBs apart from the two denoted. The references for the optical and radio measurements along with the age column that signifies the approximate time elapsed since the detection of the burst. Redshifts, z, are also given where available. If no reference for z is stated then the value is taken from one of the measurement references, the stated references are as follows: [1] Lamb et al. (1999); [2] Djorgovski et al. (1998); [3] Djorgovski et al. (1999); [4] Vreeswijk et al. (2001); [5] Vreeswijk et al. (2006); [6] Castro et al. (2000); [7] Bloom et al. (2003); [8] Castro et al. (2001); [9] Hjorth et al. (2003); [10] Barth et al. (2003); [11] Greiner et al. (2003); [12] Kelson & Berger (2005); [13] Cenko et al. (2005); [14] Berger & Becker (2005); [15] Ledoux et al. (2005); [16] Quimby et al. (2005); [17] Mirabal & Halpern (2006); [18] Bloom et al. (2006); [19] Cenko et al. (2007); [20] Fatkhullin et al. (2007); [21] Vreeswijk et al. (2008); [22] Chornock et al. (2009a); [23] Chornock et al. (2009b); [24] Chornock et al. (2009c); [25] Cenko et al. (2009); [26] Cucchiara et al. (2009); [27] Xu et al. (2009); [28] Antonelli et al. (2010); [29] O'Meara et al. (2010); [30] Chornock et al. (2010).

GRB Name	$F_{\rm o}$ ref.	$F_{ m r}$ ref.	Age (d)	z
GRB 970508	Sokolov et al. (1998)	Frail et al. (2000b)	5	0.835
GRB 980329	Palazzi et al. (1998)	Taylor et al. (1998)	< 1	≈ 2 , or $3 \lesssim z \lesssim 5$ [1]
GRB 980519	Gal et al. (1998)	Frail et al. (2000a)	3	-
GRB 980703	Bloom et al. (1998)	Frail et al. (2003b)	1	0.966[2]
GRB 990123	Castro-Tirado et al. (1999)	Kulkarni et al. (1999)	1	1.600 [3]
GRB 990510	Harrison et al. (1999)	Harrison et al. (1999)	1	1.619 [4]
GRB 991208	Castro-Tirado et al. (2001)	Galama et al. (2000)	1	0.706
GRB 991216	Jensen et al. (1999)	Frail et al. (2000c)	2	1.02[5]
GRB 000131	Andersen et al. (2000)	Frail et al. (2003a)	8	4.500
GRB $000301C$	Veillet (2000)	Berger et al. (2000)	4	2.034[6]
GRB 000418	Berger et al. (2001)	Berger et al. (2001)	11	1.118 [7]
GRB 000911	Price et al. (2002c)	Price et al. (2002c)	4	1.059
GRB 000926	Fynbo et al. (2001)	Harrison et al. (2001)	3	2.038
GRB 010222	Sagar et al. (2001)	$RADW^a$	1	1.477[8]
GRB 010921	Price et al. (2002a)	Price et al. (2002a)	26	0.451
GRB 011121	Garnavich et al. (2003)	Price et al. (2002b)	4	0.362
GRB 020124	Berger et al. (2002b)	Berger et al. (2002b)	2	3.200 [9]
GRB 020405	Masetti et al. (2003)	Berger et al. (2003b)	1	0.691
GRB 020813	Covino et al. (2003)	Frail & Berger (2002)	1	1.255 [10]
GRB 030115	Levan et al. (2006)	Frail & Berger (2003)	2	~ 2.500
GRB 030329	Lipkin et al. (2004)	Berger et al. (2003a)	< 1	0.169 [11]
GRB 050315	Cobb & Bailyn (2005)	Berger et al. (2005b)	1	1.949 [12]
GRB 050401	Watson et al. (2006)	Soderberg (2005)	5	2.899
GRB $050525A$	Della Valle et al. (2006)	Cameron & Frail $(2005)^b$	3	0.606
GRB 050603	Grupe et al. (2006)	Cameron (2005)	< 1	2.821 [14]
GRB 050724^{c}	Malesani et al. (2007)	Berger et al. (2005a)	< 1	0.257
GRB $050820A$	Cenko et al. (2006)	Cenko et al. (2006)	< 1	2.615 [15]
GRB $051109A$	Misra et al. (2005)	Frail, Cameron & Soderberg (2005)	1	2.346 [16]
GRB 051221 A^c	Soderberg et al. (2006b)	Soderberg et al. (2006b)	1	0.546
GRB 060218	Ferrero et al. (2006)	Soderberg et al. (2006a)	2	0.033[17]
GRB 061121	Halpern, Mirabal & Armstrong (2006)	Chandra & Frail (2006)	1	1.314 [18]
GRB 070125	Updike et al. (2008)	Updike et al. (2008)	2	1.547
GRB 071003	Perley et al. (2008)	Perley et al. (2008)	2	1.604
GRB $071010B$	Kann, Hoegner & Filgas (2007)	Chandra & Frail (2007a)	3	0.947 [19]
GRB 071020	Im, Lee & Urata (2007)	Chandra & Frail (2007b)	2	2.142[20]
GRB $080319B$	Bloom et al. (2009)	Soderberg, Chandra & Frail (2008)	2	0.937[21]
GRB $080603A$	Guidorzi et al. (2011)	Chandra & Frail (2008a)	2	1.687
GRB 080810	Page et al. (2009)	Chandra & Frail (2008b)	4	3.355
GRB $081203B$	Perley & Bloom (2008)	Chandra & Frail (2008c)	5	-
GRB 090313	Melandri et al. (2010)	Melandri et al. (2010)	6	3.375[22]
GRB 090323	Perley (2009a)	Harrison et al. (2009)	5	3.570 [23]
GRB 090424	Im et al. (2009)	Chandra & Frail (2009a)	2	0.544 [24]
GRB 090618	Rumyantsev & Pozanenko (2009)	Chandra & Frail (2009b)	1	0.540 [25]
GRB $090902B$	Pandey et al. (2010)	van der Horst et al. (2009)	2	1.822 [26]
GRB 091020	Perley (2009b)	Frail, Chandra & Singh (2009)	1	1.71 [27]
GRB 100418A	Moody et al. (2010)	Moin et al. (2013)	2	0.624 [28]
GRB 100814A	Nardini et al. (2014)	Chandra, Frail & Cenko (2010)	4	1.440 [29]
GRB 100901A	Rumyantsev, Shakhovkoy & Pozanenko (2010)	van der Horst et al. (2010)	3	1.408 [30]

^a Measurement taken from the 'Radio Afterglow Data Website' (RADW; http://www.aoc.nrao.edu/~dfrail/allgrb_table.shtml).

 $[^]b$ Closer measurement in time taken from RADW.

^c Short GRB.

26 Stewart et al.

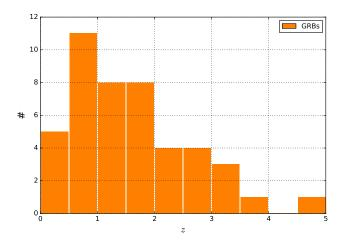


Figure A4. The distribution of redshifts of the GRB sample. Refer to Table A5 for the references of the redshift measurements.